

## LA-UR-21-30101

Approved for public release; distribution is unlimited.

Title:	Physics Informed Machine Learning of SPH: Machine Learning Lagrangian Turbulence
Author(s):	Woodward, Michael Joseph Tian, Yifeng Hyett, Criston Matthew Fryer, Christopher Lee Livescu, Daniel Stepanov, M. Chertkov, Michael
Intended for:	Web
Issued:	2021-10-12 (Draft)

---

**Disclaimer:**

Los Alamos National Laboratory, an affirmative action/equal opportunity employer, is operated by Triad National Security, LLC for the National Nuclear Security Administration of U.S. Department of Energy under contract 89233218CNA000001. By approving this article, the publisher recognizes that the U.S. Government retains nonexclusive, royalty-free license to publish or reproduce the published form of this contribution, or to allow others to do so, for U.S. Government purposes. Los Alamos National Laboratory requests that the publisher identify this article as work performed under the auspices of the U.S. Department of Energy. Los Alamos National Laboratory strongly supports academic freedom and a researcher's right to publish; as an institution, however, the Laboratory does not endorse the viewpoint of a publication or guarantee its technical correctness.

# Physics Informed Machine Learning of SPH: Machine Learning Lagrangian Turbulence

Michael Woodward<sup>\*1</sup>, Yifeng Tian<sup>†2</sup>, Criston Hyett<sup>‡1</sup>, Chris Fryer<sup>§2</sup>, Daniel  
Livescu<sup>¶2</sup>, Mikhail Stepanov<sup>||1</sup> and Michael Chertkov<sup>\*\*1</sup>

<sup>1</sup>Graduate Interdisciplinary Program in Applied Mathematics, Department of  
Mathematics, University of Arizona, Tucson, AZ 85721

<sup>2</sup> Computer, Computational and Statistical Sciences Division, Los Alamos  
National Laboratory, Los Alamos, NM 87544

March 2, 2022

## Abstract

Smoothed particle hydrodynamics (SPH) is a mesh-free Lagrangian method for obtaining approximate numerical solutions of the equations of fluid dynamics; which has been widely applied to weakly- and strongly compressible turbulence in astrophysics and engineering applications. We present a learn-able hierarchy of parameterized and "physics-explainable" Lagrangian based fluid simulators using both physics based parameters and Neural Networks (NNs) as universal function approximators. This hierarchy of parameterized Lagrangian models gradually introduces more SPH based structure, which we show improves interpretability, generalizability (over larger ranges of time scales and Mach numbers), preservation of physical symmetries (corresponding to conservation of linear and angular momentum), and requires less training data. Our learning algorithm develops a mixed mode approach, mixing forward and reverse mode automatic differentiation with local sensitivity analyses to efficiently perform gradient based optimization. We train this hierarchy on both weakly compressible SPH and DNS data, and show that our physics informed learning method is capable of: (a) solving inverse problems over the physically interpretable parameter space, as well as over the space of NN parameters; (b) learning Lagrangian statistics of turbulence (interpolation);

---

\*mwoodward@math.arizona.edu

†yifengtian@lanl.gov

‡cmhyett@math.arizona.edu

§fryer@lanl.gov

¶livescu@lanl.gov

||stepanov@math.arizona.edu

\*\*chertkov@math.arizona.edu

(c) combining Lagrangian trajectory based, probabilistic, and Eulerian field based loss functions; (d) extrapolating beyond training sets into more complex regimes of interest; (e) learning new parameterized smoothing kernels better suited to weakly compressible DNS turbulence data.

## Contents

<b>1</b>	<b>Introduction</b>	<b>3</b>
<b>2</b>	<b>Related Work</b>	<b>5</b>
<b>3</b>	<b>Smoothed Particle Hydrodynamics</b>	<b>6</b>
3.1	Approximation of Equations of Motion . . . . .	6
3.2	Example Flow: SPH Training Set . . . . .	7
<b>4</b>	<b>Mixed Mode Physics Informed Machine Learning Methods</b>	<b>7</b>
4.1	Hierarchy of models . . . . .	8
4.1.1	Parameterized Smoothing Kernel . . . . .	10
4.2	Mixing Sensitivity Analysis and Automatic Differentiation . . . . .	10
4.2.1	Forward and Adjoint based Methods . . . . .	11
4.3	Mixed Mode AD . . . . .	12
4.4	Loss functions . . . . .	12
4.4.1	Trajectory Based Loss Function . . . . .	12
4.4.2	Field Based Loss Function . . . . .	13
4.4.3	Lagrangian Statistics Based Loss Function . . . . .	13
4.5	Performance comparison . . . . .	13
<b>5</b>	<b>Results: Evaluating and Testing Models on SPH data</b>	<b>14</b>
5.1	Results: Interpolation of Models . . . . .	14
5.2	Results: Generalizability (extrapolation capability) on SPH flow data . . .	15
<b>6</b>	<b>Results: Evaluating and Testing Models on DNS data</b>	<b>21</b>
6.1	DNS data . . . . .	22
6.2	Comparing Smoothing Kernels . . . . .	22
6.3	Comparing Equations of State . . . . .	22
6.4	Generalizability . . . . .	25
<b>7</b>	<b>Conclusions</b>	<b>30</b>
7.1	Future work . . . . .	30
<b>8</b>	<b>Reproducibility Statement</b>	<b>31</b>

<b>A Appendix: SPH (in more details)</b>	<b>36</b>
A.1 Basic formulation . . . . .	36
A.2 Approximation of Flow Equations . . . . .	38
A.3 External Forcing . . . . .	40
A.4 Numerical Algorithm for Forward Solving SPH . . . . .	41
<b>B Appendix: Methods</b>	<b>41</b>
B.0.1 Forward Sensitivity Analysis . . . . .	41
B.0.2 Adjoint Method . . . . .	43
B.1 Learning Algorithm . . . . .	46
<b>C Additional SPH training data Results</b>	<b>46</b>
<b>D Additional DNS results: Training on <math>M_t = 0.16</math></b>	<b>47</b>

## 1 Introduction

**Why turbulence? Why Lagrangian?** Understanding turbulent flows is crucial for many engineering and scientific fields, and remains a great unresolved challenge of classical physics Frisch (1995). Many computational fluid dynamics (CFD) approaches Harlow (2004) are being explored in this direction by numerically approximating the Navier-Stokes (NS) equations, which are well established in the field as explaining the "ground truth". One such CFD approach is the mesh-free Smoothed Particle Hydrodynamics (SPH) method Gingold & Monaghan (1977); Monaghan (1992, 2012), which has been widely applied to weakly- and strongly compressible turbulence in astrophysics and many engineering applications Shadloo et al. (2016). It is one of a small set of approaches based on a Lagrangian construction: fluid quantities follow the flow using particles as opposed to the Eulerian approach which computes flow quantities at fixed locations on a computational mesh. This mesh-free, Lagrangian approximation of NS is appealing because it naturally un.masks correlations at the resolved scale from sweeping by larger scale eddies Kraichnan (1964, 1965), therefore suggesting a more natural setting for understanding advection dominated flows, mixing and dispersion, and turbulent transport. Developing approximation-optimal SPH models (and simulators) for turbulent flows is an ongoing area of research Lind et al. (2020), to which this paper contributes. Specifically, we show how modern tools of machine learning and applied mathematics, such as NNs, automatic differentiation (AD), and local sensitivity analysis (SA), can be utilized to learn and design better SPH models; such as learning new smoothing kernels, a key ingredient in the SPH construction.

**Physics Informed Machine Learning: What and Why?** Numerical simulators, including CFD, have recently blended with modern machine learning tools Ling et al. (2016); King et al. (2018); Schenck & Fox (2018); Mohan & Gaitonde (2018); Duraisamy et al. (2019); Fonda et al. (2019); Mohan et al. (2020a); Maulik et al. (2020); Ummenhofer et al. (2020); Mohan et al. (2020b); Tian et al. (2021) out of which a promising field,

coined Physics Informed Machine Learning (PIML), is emerging (and being re-discovered Lagaris et al. (1998)). As set, some eight years ago at the first LANL workshop with this name CNLS at LANL (2016, 2018, 2020), PIML was meant to pivot the mixed community of machine learning researchers on the one hand and scientists and engineers on the other, to discover physical phenomena/models from data. Today, PIML researchers are focused on incorporating known physical structures (such as conservation laws), physical hypothesis and physical equations (and/or their numerical schemes/algorithms) into modern machine learning tools. This development is exciting for physicists, as it integrates centuries of scientific discovery with modern machine learning – boosting new ideas and resurrecting interesting but forgotten hypotheses from the past. The overall goal of PIML is two-fold King et al. (2018): learning new physics from data (experimental or computational) and improving/developing machine learning algorithms by incorporating ideas from physics (especially in what concerns explainable, interpretable, and generalizable models).

**Our Contribution: PIML for SPH.** The aim of this work is to develop learn-able Lagrangian simulators to discover physics informed models for turbulent flows at coarse grained scales. A priori we do not know which Lagrangian based model will best fit the data and generalize to other flow regimes. Thus, we develop a learn-able hierarchy of parameterized "physics-explainable" Lagrangian and SPH based fluid models that gradually includes more physical (SPH-based) structure, ranging from a Neural ODE based model Chen et al. (2019) to a weakly compressible SPH formulation (with 8 trainable and physically interpretable parameters including a new parameterized smoothing kernel). These models are trained and analyzed on both weakly compressible SPH and DNS flow data. We train these models with gradient descent using modern optimizers (e.g Adam Kingma & Ba (2017)), and mixing automatic differentiation (both forward and reverse mode) with local sensitivity analyses (such as forward and adjoint based methods). Utilizing these models and methods we show that, for the weakly compressible case, adding SPH informed structure improves interpretability, generalizability, and requires less training data compared to less informed models (such as Neural ODE). Additionally, we develop a new parameterized and learn-able smoothing kernel, which when included in the fully informed SPH based model performs the best at generalizing to different DNS flows. Furthermore, we show that the learned models are able to reconstruct the Lagrangian statistics of the flow, and can be used to learn unknown, or missing, functions embedded within SPH models by using NNs as function approximators Hornik et al. (1989).

**Outline.** The overall outline of the remainder of the manuscript is as follows. First, in section 2, an overview of related studies is given that draws connections of this manuscript to the broader field of PIML. Next, in section 3 (and in more detail Appendix A) a weakly compressible formulation of SPH is presented, which provides the basis for our work on learning Lagrangian models of turbulence using parameterized and learn-able SPH simulators. In section 4 and Appendix B, a detailed description of the learning algorithms, loss functions, and hierarchy of models are suggested, which provides the necessary tools to learn parameters of our Lagrangian based models from

data. In section 5 we train on SPH data to verify the learning algorithm and analyze the effect of incrementally adding physical structure in the hierarchy of models on a "clean" data-set (where the underlying parameters are known). Then, in section 6 we train the hierarchy of models on "real-world" weakly compressible (low turbulent Mach number) DNS data and compare each models ability to generalize to different turbulent Mach numbers and longer time scales. Finally, in section 7, we draw conclusions on the progress made so far along with providing a discussion of future work.

## 2 Related Work

Early works of incorporating scientific domain knowledge (in the form of differential equations) within deep learning algorithms dates back to the 1990s (Lagaris et al., 1998). However, in the context of modern deep learning, interest in this area has been revived (Raissi et al., 2017; Chen et al., 2019; Rackauckas et al., 2020; Ladický et al., 2015). In part, this is due to the increased computational power afforded by parallelism across both CPUs and GPUs, along with notable achievements across disciplines (such as scientific applications (Zhai et al., 2020), data-compression algorithms (Wang et al., 2016), computer vision (Serre, 2019), and natural language processing (Deng & Liu, 2018)). The main computational utilities and strategies of physics informed learning includes embedding physical structure into learn-able models, applying NNs as function approximators (Hornik et al., 1989), differential programming using automatic differentiation (Rackauckas et al., 2020; Bücker, 2006), and optimization tools to minimize an objective function.

There are several approaches that can be taken to develop a PIML algorithm; (1) enforcing soft constraints by adding physical structure, or symmetries into the loss function (as was done in (Raissi et al., 2017) where Neural Networks are used to discover and solve parameterized PDEs from data); (2) enforce physical constraints directly into the NN architecture (such as in (Mohan et al., 2020a) enforced the incompressibility constraint into a Convolutional NN); (3) utilize NN's as function approximators along with physical parameters/structure embedded within differentiable numerical simulators (as was done in (Chen et al., 2019; Rackauckas et al., 2020; Tian et al., 2021)); (4) mixing differentiable programming with SA along with physical structure and NNs as was done by (Ma et al., 2021; Chen et al., 2019) (which from a technical perspective is most related to our work). The methods of this work is most related to (4) as *an approach to build parameterized Lagrangian models for turbulence. However, in this manuscript, we combine these scientific disciplines to not only provide a tool for approaching the discovery of optimal Lagrangian and SPH based models of turbulence, but also to explore the effects of adding physical structure into ML algorithms on extrapolation and generalizability.*

In recent years, there have been several works that have integrated ML and DL techniques for Lagrangian flows. The pioneering work by (Ladický et al., 2015) used SPH related models and regression forests along with physics informed feature vectors, demonstrating that flow representations can be learned with data-driven techniques. In (de Anda-Suárez et al., 2018), evolutionary algorithms are applied for optimization

of parameters in SPH flows. Further works began utilizing differentiable programming techniques, such as in (Schenck & Fox, 2018) for robotic control for pouring applications and in (Ummenhofer et al., 2020) where a continuous convolutional neural network operation is developed on unordered particle data for learning and simulating SPH. (Tian et al., 2021) learns reduced models describing the Lagrangian dynamics of the velocity gradient tensor from Direct Numerical Simulation data. Other works have used experimental data from Particle Image Velocimetry and NNs to track particles embedded in a flow (Rabault et al., 2017; Lee et al., 2017; Cai et al., 2019; Stulov & Chertkov, 2021).

### 3 Smoothed Particle Hydrodynamics

One of the most prominent particle-based Lagrangian methods for obtaining approximate numerical solutions of the equations of fluid dynamics is Smoothed Particle Hydrodynamics (SPH) Monaghan (2005). Originally introduced independently by Lucy (1977) and Gingold & Monaghan (1977) for astrophysical flows, however, over the following decades, SPH has found a much wider range of applications including computer graphics, free-surface flows, fluid-structure interaction, bioengineering, compressible flows, galaxies' formation and collapse, high velocity impacts, geological flows, magnetohydrodynamics, and turbulence Lind et al. (2020); Shadloo et al. (2016). Below, we give a brief formulation of SPH and in subsection 4.1 we hard code SPH structure into a hierarchy of "physics-explainable" models.

#### 3.1 Approximation of Equations of Motion

Essentially, SPH is a discrete approximation to a continuous flow field by using a series of discrete particles as interpolation points (using an integral interpolation with smoothing kernel  $W$ ). Using the SPH formalism the partial differential equations (PDEs) of fluid dynamics can be approximated by a system of ordinary differential equations (ODEs) for each particle (indexed by  $i$ ),  $\forall i \in \{1, 2, \dots, N\}$  :

$$\frac{d\mathbf{r}_i}{dt} = \mathbf{v}_i, \quad (1)$$

$$\frac{d\mathbf{v}_i}{dt} = - \sum_{j \neq i}^N m_j \left( \frac{P_j}{\rho_j^2} + \frac{P_i}{\rho_i^2} + \Pi_{ij} \right) \nabla_i W_{ij} + \mathbf{f}_{ext}. \quad (2)$$

Where  $W_{ij} = W(\|\mathbf{r}_i - \mathbf{r}_j\|, h)$ ,  $P_i$ , and  $\rho_i$  represents pressure and density (respectively) at particle  $i$ .  $\Pi_{ij}$  is an artificial viscosity term Monaghan (2012) used to approximate the viscous terms. Density and pressure (for the weakly compressible formulation) are computed by

$$\rho_i = \sum_j m_j W(|\mathbf{r}_i - \mathbf{r}_j|, h), \quad (3)$$

$$P(\rho) = \frac{c^2 \rho_0}{\gamma} \left[ \left( \frac{\rho}{\rho_0} \right)^\gamma - 1 \right]. \quad (4)$$

See Appendix A for a more detailed derivation, which follows Monaghan (2012). Briefly, Eq. (2) is an approximation of Euler’s equations for weakly compressible flows, with an added artificial viscosity term  $\Pi_{ij}$ . In this manuscript, deterministic and stochastic external forcing  $f_{ext}$  were explored, which provides the energy injection mechanism. We also utilize the popular formulation of an artificial viscosity  $\Pi_{ij}$  described in Eq. (20), which approximates in aggregate contributions from the bulk and shear viscosity ( $\alpha$ ), a Nueman-Richtmyer viscosity for handling shocks ( $\beta$ ) Monaghan (2012); Morris et al. (1997), as well as the effective, eddy viscosity effect of turbulent advection from the under-resolved scales, i.e. scales smaller than the mean-particle distance.

### 3.2 Example Flow: SPH Training Set

Fig. (1) shows consecutive snapshots of an exemplary multi-particle SPH flow in three dimensional space, where coloration is added for visualization purposes. We use a standard set of parameters for weakly-compressible flows (see Cossins (2010))  $\alpha = 1.0$  (bulk-shear viscosity),  $\beta = 2\alpha$  (Nueman-Richtmyer viscosity),  $c = 10$ ,  $\gamma = 7.0$  with energy injection rate  $\theta = 0.5$ , and deterministic external forcing, (see Appendix A for more details on the parameters and equations such as the equation of state and artificial viscosity). The inverse problem we pose consists in the following; given a sequence of snapshots of SPH particle flows, estimate the parameters of the SPH model (a hierarchy of which is discussed in subsection 4.1) that best fits the SPH flow data over a predefined time scale.

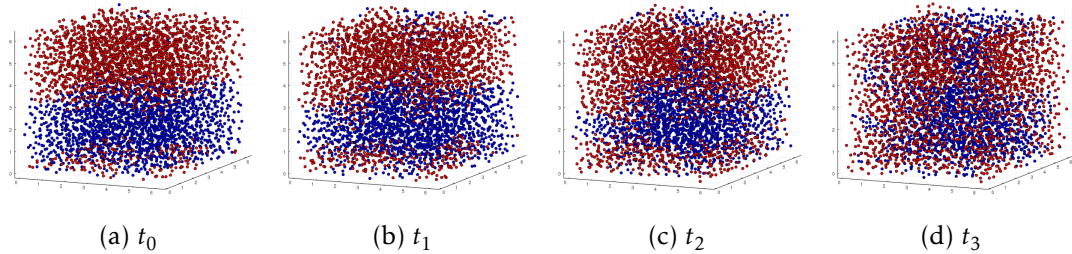


Figure 1: SPH particles advancing in time driven by external forcing  $f_{ext}$  (as described in Appendix A) used as training data, where coloration is added for visualization purposes and  $t_{i+1} - t_i \approx 50\Delta t$ .

## 4 Mixed Mode Physics Informed Machine Learning Methods

This section includes the hierarchy of parameterized SPH informed models, methods for computing the gradients, and formulating the loss functions. We give a brief

overview of our mixed mode physics informed learning algorithm (a first order gradient based optimization approach). These methods are implemented using the open source software Julia (Bezanson et al., 2017), which is a fast and flexible dynamic language, appropriate for high performance scientific and numerical computing, along with a wide range of data science and machine learning packages such as Flux.jl (Innes et al., 2018), and AD packages Zygote.jl (Innes, 2018), ForwardDiff.jl (Revels et al., 2016). For a more detailed treatment on our learning algorithms (1) (including derivations), and loss functions see Appendix B.

#### 4.1 Hierarchy of models

We develop a hierarchy of parameterized Lagrangian models that gradually includes more SPH based structure. The motivation for this is twofold: (1) systematically analyze the effect of including more physical structure, and (2) a priori, we do not know which Lagrangian model will best fit the DNS ground truth data, as well as generalize to different flow regimes not seen in training. Multilayer Perceptrons (MLPs) with hyperbolic tangent activation functions are used as a universal function approximators (Hornik et al., 1989) embedded within an ODE structure describing the Lagrangian flows. It was found through hyper-parameter tuning that 2 hidden layers were sufficient for each model using a NN. Each of the models below evolve the position of the particles according to

$$\frac{d\mathbf{r}_i}{dt} = \mathbf{v}_i \quad \forall i = 1, \dots, N,$$

where the acceleration operator is uniquely parameterized.

- **NODE:** In this least informed (and most flexible) Neural ODE Chen et al. (2019) based model, the entire acceleration operator is approximated by a NN, with the exception of  $\mathbf{f}_{ext}$ . This is most related to the work done by (Chen et al., 2019). We make an additional modification by considering the interaction of particles to be within a local cloud (using the cell linked list algorithm (Domínguez et al., 2011)). Note that no pairwise interaction between particles is assumed. We assume that velocities,  $\mathbf{v}_i(t)$ , and coordinates,  $\mathbf{r}_i(t)$ , of  $N$  particles evolve in time according to

$$\frac{d\mathbf{v}_i}{dt} = \text{NN}_{\theta}(\mathbf{r}_{ij}, \mathbf{v}_{ij} | \forall j : \|\mathbf{r}_{ij}\| \leq 2h) + \mathbf{f}_{ext}(\theta_{inj}), \quad (5)$$

where  $\mathbf{r}_{ij} = \mathbf{r}_i - \mathbf{r}_j$ ,  $\mathbf{v}_{ij} = \mathbf{v}_i - \mathbf{v}_j$ ,  $\text{NN}_{\theta} : \mathbb{R}^{2dm} \rightarrow \mathbb{R}^l \rightarrow \mathbb{R}^l \rightarrow \mathbb{R}^d$  ( $d = 2, 3$  is the space dimension,  $m$  is the fixed number of particles that are closest to the  $i$ -th particle in each cloud, and  $l$  is the height, or number of nodes, of the hidden layer). Although this NN is approximating a function which is interpretable (acceleration), the individual parameters of the NN are not. With some tuning, it was found that  $m \in \{20, 21, \dots, 30\}$  and  $l \in \{5, 6, \dots, 12\}$  generally produce the best fit.  $\theta$  and  $\theta_{inj}$  are the trainable parameters.

- **NN summand:** In the direction of including more of the SPH based physical structure, pairwise interaction is assumed represented via a sum over the  $i$ -th particle neighborhood, where the summand term is approximated by a NN. Here, Eq. (2) is modeled

by the Lagrangian based ODE

$$\frac{d\mathbf{v}_i}{dt} = \sum_j^N \mathbf{NN}_\theta(\mathbf{r}_{ij}, \mathbf{v}_{ij}) + \mathbf{f}_{ext}(\theta_{inj}), \quad (6)$$

where  $\mathbf{NN}_\theta : \mathbb{R}^{2d} \rightarrow \mathbb{R}^l \rightarrow \mathbb{R}^l \rightarrow \mathbb{R}^d$ . With some tuning,  $l \in \{5, 6, \dots\}$  generally produce the best fit.  $\theta$  and  $\theta_{inj}$  are the trainable parameters.

• **Rotationally Invariant NN:** In this formulation, built on the top of the NN summand, we use a neural network of the form  $\mathbf{NN}_\theta : \mathbb{R}^4 \rightarrow \mathbb{R}^l \rightarrow \mathbb{R}^l \rightarrow \mathbb{R}$  to approximate the pair-wise part of the acceleration term in Eq. (2), where the rotational invariance is hard coded by construction (about a rotationally invariant basis expansion using the difference vector  $\mathbf{r}_{ij}$ )

$$\frac{d\mathbf{v}_i}{dt} = \sum_j^N \mathbf{NN}_\theta \left( \frac{P_i}{\rho_i^2}, \frac{P_j}{\rho_j^2}, \mathbf{r}_{ij} \cdot \mathbf{v}_{ij}, \|\mathbf{r}_{ij}\|_2 \right) \mathbf{r}_{ij} + \mathbf{f}_{ext}(\theta_{inj}). \quad (7)$$

With some tuning,  $l \in \{5, 6, \dots\}$  generally produce the best fit.  $\theta$  and  $\theta_{inj}$  are the trainable parameters.

•  **$\nabla P$ -NN:** Next, we push the neural network deeper within the summand term and now explicitly include the  $\Pi$ -, i.e. artificial viscosity term, and use a NN to approximate the gradient of pressure contribution (i.e  $\nabla P$ - term in SPH Eq. (2), see Appendix A for more details):

$$\frac{d\mathbf{v}_i}{dt} = - \sum_j^N m_j (\mathbf{NN}_\theta(\mathbf{r}_{ij}) + \Pi_{ij}(\alpha, \beta)) \nabla W_{ij}(r; h) + \mathbf{f}_{ext}(\theta_{inj}), \quad (8)$$

where  $\mathbf{NN}_\theta : \mathbb{R}^d \rightarrow \mathbb{R}^l \rightarrow \mathbb{R}^l \rightarrow \mathbb{R}$ .  $l \in \{5, 6, \dots\}$  generally produce the best fit.  $\theta$ ,  $\alpha$ ,  $\beta$  and  $\theta_{inj}$  are the trainable parameters.

• **EqS NN:** Approximating the equation of state with a NN in the weakly compressible SPH formulation:

$$\frac{d\mathbf{v}_i}{dt} = - \sum_j^N m_j \left( \frac{P_{nn\theta}(\rho_i)}{\rho_i^2} + \frac{P_{nn\theta}(\rho_j)}{\rho_j^2} + \Pi_{ij}(\alpha, \beta) \right) \nabla W_{ij}(r; h) + \mathbf{f}_{ext}(\theta_{inj}). \quad (9)$$

where  $P_{nn\theta}(\rho) : \mathbb{R} \rightarrow \mathbb{R}^l \rightarrow \mathbb{R}^l \rightarrow \mathbb{R}$ .  $l \in \{8, 9, \dots, 12\}$  generally produce the best fit.  $\theta$ ,  $\alpha$ ,  $\beta$  and  $\theta_{inj}$  are the trainable parameters.

• **Fully Physics Informed: Fixed smoothing Kernel** In this formulation, the entire weakly compressible SPH structure is used, and the physically interpretable parameters  $\alpha, \beta, \gamma, c, p_0, \theta_{inj}$  are learned

$$\frac{d\mathbf{v}_i}{dt} = - \sum_j^N m_j \left( \frac{P_i(c, \gamma, p_0)}{\rho_i^2} + \frac{P_j(c, \gamma, p_0)}{\rho_j^2} + \Pi_{ij}(\alpha, \beta) \right) \nabla W_{ij}(r; h) + \mathbf{f}_{ext}(\theta_{inj}). \quad (10)$$

• **Fully Physics Informed: Parameterized  $W$**  In this formulation, the entire weakly compressible SPH structure is used along with a novel parameterized smoothing kernel, and the physically interpretable parameters  $\alpha, \beta, \gamma, c, a, b, \theta_{inj}$  are learned ( $a, b$  are parameters defined below in subsection 4.1.1 for a parameterized smoothing kernel).

$$\frac{dv_i}{dt} = - \sum_j m_j \left( \frac{P_i(c, \gamma, p_0)}{\rho_i^2} + \frac{P_j(c, \gamma, p_0)}{\rho_j^2} + \Pi_{ij}(\alpha, \beta) \right) \nabla W_{ij}(r; h, a, b) + f_{ext}(\theta_{inj}). \quad (11)$$

We note that as more of the physics informed SPH based structure is added into the learning algorithm, the learned models become more interpretable; i.e. the learned parameters are associated with actual physical quantities.

#### 4.1.1 Parameterized Smoothing Kernel

Eq. (11) depends on a smoothing kernel. We introduce the following parameterized smoothing kernel

$$W(r; h, a, b) = \begin{cases} \sigma(1 - (r/(2h))^a)^b, & 0 \leq r < 2h \\ 0, & \text{otherwise} \end{cases}, \quad (12)$$

where,  $r = |\mathbf{r}|$ ,  $h$  sets the spatial scale (of coarse-graining), and constant,  $\sigma$ , dependent on the parameters  $a, b$  and the problem dimensionality, is chosen to guarantee normalization,  $\int d\mathbf{r} W(r; h, a, b) = 1$ , thus

$$\sigma_{2D} = \frac{\Gamma(b + 2/a + 1)}{4\pi h^2 \Gamma(b + 1) \Gamma(2/a + 1)},$$

$$\sigma_{3D} = \frac{3\Gamma(b + 3/a + 1)}{32\pi h^3 \Gamma(b + 1) \Gamma(3/a + 1)}.$$

## 4.2 Mixing Sensitivity Analysis and Automatic Differentiation

Sensitivity analysis (SA) is a classical technique found in many applications, such as gradient-based optimization, optimal control, parameter identification, model diagnostics, (see (Donello et al., 2020) and many historical references there in). Also, local SA was recently utilized to learn neural network parameters within ODEs (Chen et al., 2019; Rackauckas et al., 2020; Ma et al., 2021). In the context of this work, we use local SA to form the main computational algorithm for computing gradients of a loss function with respect to the parameters within the hierarchy of Lagrangian models. Within the SA framework, we apply Automatic Differentiation (AD) (see (Ma et al., 2021; Bücker, 2006) and references there in); such as forward mode and reverse mode AD to compute derivatives, where the method is chosen based on efficiency, which depends on the dimension of the input and output space of the function being differentiated. The losses used in this work are defined in Eq. (4.4), but in general, we consider

loss functions of the form,  $L(\mathbf{X}, \boldsymbol{\theta}) = \int_0^{t_f} \Psi(\mathbf{X}, \boldsymbol{\theta}, t) dt$ , where  $\mathbf{X}$  and  $\boldsymbol{\theta}$  are, respectively, the matrix of states (particles coordinates and velocities) and the vector of parameters introduced in the next subsection.  $\Psi$  is some measure of performance at time  $t$  (see the following subsection 4.4 for more details).

#### 4.2.1 Forward and Adjoint based Methods

Let us, first, introduce some useful notations for our parameterized SPH informed models;  $\mathbf{X}_i = (\mathbf{r}_i, \mathbf{v}_i)^T$ ,  $\mathbf{X} = \{\mathbf{X}_i | i = 1, \dots, N\}$ , where,  $\mathbf{r}_i = (x_i, y_i, z_i)$ , and,  $\mathbf{v}_i = (u_i, v_i, w_i)$ , are the position and velocity of particle  $i$  respectively. Also,  $\boldsymbol{\theta} = [\theta^1, \dots, \theta^p]^T$  where  $p$  is the number of model parameters. Now, each parameterized Lagrangian model in the hierarchy can be stated in the ODE form

$$\forall i: \quad d\mathbf{X}_i/dt = \mathcal{F}_i(\mathbf{X}(t, \boldsymbol{\theta}), \boldsymbol{\theta}) = (\mathbf{v}_i, \mathbf{F}_i(\mathbf{X}, \boldsymbol{\theta}))^T, \quad (13)$$

where  $\mathbf{F}_i(\mathbf{X}, \boldsymbol{\theta}) = \dot{\mathbf{v}}_i$  is the parameterized acceleration operator as defined in the above hierarchy. Forward and Adjoint based Sensitivity Analyses (FSA, ASA), analogous to forward and reverse mode AD respectively, can be used to compute the gradient of the loss function (see Section 4.4),

$$\partial_{\boldsymbol{\theta}} L = \int_0^{t_f} \partial_{\mathbf{X}} \Psi(\mathbf{X}, \boldsymbol{\theta}, t) d_{\boldsymbol{\theta}} \mathbf{X}(\boldsymbol{\theta}, t) + \partial_{\boldsymbol{\theta}} \Psi(\mathbf{X}, \boldsymbol{\theta}, t) dt, \quad (14)$$

(for derivations of FSA and ASA see Appendix B). Briefly, FSA computes the sensitivity equations (SE) for  $\mathbf{S}_i^\alpha = d\mathbf{X}_i/d\theta^\alpha$ , by simultaneously integrating a system of ODEs:  $(\forall i, \forall \alpha = 1, \dots, p: )$

$$\frac{d\mathbf{S}_i^\alpha}{dt} = \frac{\partial \mathcal{F}_i(\mathbf{X}(t), \boldsymbol{\theta})}{\partial \mathbf{X}_i} \mathbf{S}_i^\alpha + \frac{\partial \mathcal{F}_i(\mathbf{X}(t), \boldsymbol{\theta})}{\partial \theta^\alpha} \quad (15)$$

which has a computational cost that scales linearly with the number of parameters.  $\mathbf{S}_i^\alpha$  is computed by solving the IVP Eq. (15) with the initial condition  $\mathbf{S}_i^\alpha(0) = 0$  (assuming  $\mathbf{X}(0)$  does not depend on  $\boldsymbol{\theta}$ ). After solving for  $\mathbf{S}_i^\alpha$ , the gradient is computed directly from Eq. (14) which is used with standard optimization tools (e.g. Adam Kingma & Ba (2017)) to update the model parameters iteratively to minimize the loss (see Algorithm 1). As opposed to the FSA method, the ASA approach avoids needing to compute  $d_{\boldsymbol{\theta}} \mathbf{X}$  by instead numerically solving a system of equations for the adjoint equation (AE) Eq. (25) backwards in time, according to subsection B.0.2. Once  $\boldsymbol{\lambda}$  is computed through integration backwards in time, the gradient of the loss function can be computed according to,  $\partial_{\boldsymbol{\theta}} L = -\int_0^{t_f} \boldsymbol{\lambda}^T \partial \mathcal{F} / \partial \boldsymbol{\theta} dt$ . The computational cost of solving the AE is independent of the number of parameters, however, for high dimensional time dependent problems, the forward-backward workflow of solving the AE imposes a significant storage cost since the AE must be solved backwards in time (Donello et al., 2020; Nouri et al., 2022). In this work, we explored both the FSA and ASA methods,

and found that the FSA was more efficient for our high dimensional time dependent problem with the number of parameters relatively small (it was found through hyperparameter tuning that the number of parameters  $\mathcal{O}(1) \lesssim p \lesssim \mathcal{O}(9 * 10^2)$  for the best fit models within the hierarchy of this work).

### 4.3 Mixed Mode AD

In both FSA and ASA described above, the gradient of  $\mathcal{F}_i$  with respect to the parameters,  $\partial \mathcal{F}_i(\mathbf{X}(\tau), \boldsymbol{\theta}) / \partial \boldsymbol{\theta}$ , and the Jacobian matrix,  $\{\partial \mathcal{F}_i(\mathbf{X}(\tau), \boldsymbol{\theta}) / \partial \mathbf{X}_j | \forall i, j\}$ , need to be computed. In this manuscript, we accomplish this with a mixed mode approach, i.e. mixing forward and reverse mode AD, where the choice is based on efficiency. Depending on the model used, many of the functions to be differentiated have varying input and output dimensions. For example, when computing  $\partial \mathcal{F}_i(\mathbf{X}(\tau), \boldsymbol{\theta}) / \partial \theta^\alpha$ , with AD where,  $\mathcal{F}_i(\boldsymbol{\theta}) : \mathbb{R}^p \rightarrow \mathbb{R}^{2d}$ , if  $p \gg 2d$ , then reverse mode AD is more efficient than forward mode (Bücker, 2006).

### 4.4 Loss functions

In this section, we construct three different loss functions: trajectory based (Lagrangian), field based Eulerian, and Lagrangian statistics based, described in the following three subsections. Since our overall goal involves learning Lagrangian and SPH based models for turbulence applications, it is the underlying statistical features and large scale field structures we want our models to learn and generalize with. This is discussed further in section 5 and section 6, where we compare the statistical and field based generalizability of each model within the hierarchy.

#### 4.4.1 Trajectory Based Loss Function

A simple loss function to consider is the Mean Squared Error (*MSE*) of the difference in the Lagrangian particles positions and velocities, as they evolve in time,

$$L_{tr}(\boldsymbol{\theta}) = MSE(\mathbf{X}, \hat{\mathbf{X}}(\boldsymbol{\theta})) = \|\mathbf{X} - \hat{\mathbf{X}}(\boldsymbol{\theta})\|^2 / N,$$

where  $\mathbf{X}$  and  $\hat{\mathbf{X}}$  are the particle states – the ground truth and the predicted, respectively. Minimizing this loss function will result in discovering optimal parameters such that the predicted trajectories gives the best possible match (within the model) for each of the particles. Notice that this "perfect" matching of the multi-particle state is not really appropriate for tracking temporal correlations in turbulence on the time scales longer than the turn-over time of the resolved eddy (estimated, roughly, as the time needed for a pair of initially neighboring particles to separate on a distance comparable to their initial separation). This is due to the fact that turbulence is intrinsically chaotic, therefore resulting in a strong sensitivity of the state (Lagrangian particle positions and velocities) on its initial conditions. Therefore, we expect the trajectory based loss method to over-fit when the observation (tracking) time is sufficiently long.

#### 4.4.2 Field Based Loss Function

The field based loss function tries to minimize the difference between the large scale structures found in the Eulerian velocity fields,

$$L_f(\boldsymbol{\theta}) = \text{MSE}(\mathbf{V}^f, \hat{\mathbf{V}}^f) = \|\mathbf{V}^f - \hat{\mathbf{V}}^f\|^2/N_f,$$

where  $\mathbf{V}_i^f = \sum_{j=1}^{N_f} (m_j/\rho_j) \mathbf{v}_j W_{ij}(\|\mathbf{r}_i^f - \mathbf{r}_j\|, h)$  uses the same SPH smoothing approximation to interpolate the particle velocity onto a predefined mesh  $\mathbf{r}^f$  (with  $N_f$  grid points). Lets recall that SPH is, by itself, an approximation for the velocity field, therefore providing a strong additional motivation for using the field based loss function.

#### 4.4.3 Lagrangian Statistics Based Loss Function

In order to approach learning Lagrangian models that capture the statistical nature of turbulent flows, one can use well established statistical tools/objects, such as single particle statistics (Yeung & Bogras, 2004). In this direction, consider the time integrated Kullback–Leibler divergence (KL) as a loss function

$$L_{kl}(\boldsymbol{\theta}) = \int_{t=0}^{t_f} \int_{-\infty}^{\infty} G_{gt}(t, \mathbf{z}_{gt}, \mathbf{x}) \log \left( \frac{G_{gt}(t, \mathbf{z}_{gt}, \mathbf{x})}{G_{pr}(t, \mathbf{z}_{pr}(\boldsymbol{\theta}), \mathbf{x})} \right) d\mathbf{x} dt,$$

where  $\mathbf{z}_{gt} = \mathbf{z}_{gt}(t)$ , and  $\mathbf{z}_{pr}(\boldsymbol{\theta}) = \mathbf{z}_{pr}(\boldsymbol{\theta}, t)$  represent single particle statistical objects over time of the ground truth and predicted data, respectively. For example, we can use the velocity increment,  $\mathbf{z}^i(t) = (\delta u_i, \delta v_i, \delta w_i)$ , where  $\delta u_i(t) = u_i(t) - u_i(0)$  and  $\mathbf{z}$  ranges over all particles. Here  $G(t, \mathbf{z}(t), \mathbf{x})$  is a continuous probability distribution (in  $\mathbf{x}$ ) constructed from data  $\mathbf{z}(t)$  using Kernel Density Estimation (KDE), to obtain smooth and differentiable distributions from data, as discussed in (Chen, 2017)), that is

$$G(\tau, \mathbf{z}, \mathbf{x}) = (Nh)^{-1} \sum_{i=1}^N K((z_i - \mathbf{x})/h),$$

where  $K$  is the smoothing kernel (chosen to be the normalized Gaussian in this work) In 3D experiments training on SPH data (discussed in the next section), we use  $L_{kl} + L_f$  as a combination of statistical and field based loss functions, with the expectation that the gradient descent (in the process of training) will drive different parameters, responsible for large and small structures, to their optimal values in unison.

#### 4.5 Performance comparison

Table 1 Shows a comparison of run-times and memory used for 2D models, applying one step of the training algorithm (see 1); where the prediction step is carried out on the time scale  $t_\lambda$  (the time scale required for a pair of neighboring particles to separate by the distance which is in average factor  $O(1)$  larger than the pair's initial separation).

Table 1: Comparing (2D) models: Run-times and Memory,  $t \sim t_\lambda$ : One iteration

Model with FSA	Run-time (s)	Memory (GiB)
NODE	15.50	9.62
NN Sum	41.60	15.61
Rot Inv	29.16	9.70
$\nabla P$	29.37	9.51
EoS NN	8.87	5.19
Phys Inf	6.03	3.52

## 5 Results: Evaluating and Testing Models on SPH data

In this section, we demonstrate the effects of incrementally embedding physical structure (known to generate the ground truth SPH data) into the Lagrangian models. We show the ability of the mixed mode FSA + AD method to learn the parameterized Lagrangian and SPH based simulators on SPH flow data (as seen in section 3) with the field based loss and a mixture of field based and statistical based loss functions. We show that each model is capable of solving the interpolation problem, which we evaluate using several quantitative and qualitative diagnostics, but as more physical structure is embedded in the model, the better is the generalizability to flows not seen in training and the better it conserves linear and angular momentum. We also notice that another important advantage of the physics informed models is that they require less training data (as seen in Figure 7) and are more efficient to train Table 1.

Each parameterized Lagrangian model within the hierarchy (see subsection 4.1) is trained under equivalent conditions: (a) on the same SPH samples (see subsection 3.2) of fixed temporal duration (which we choose to be equal to the time scale required for a pair of neighboring particles to separate by the distance which is on average a factor of  $O(1)$  larger than the pair’s initial separation and henceforth denoted  $t_\lambda$ ); (b) with the same loss function  $L_{kl} + L_f$ ; (c) with the FSA method; and (d) with a deterministic forcing  $f_{ext}$  (subsection A.3 with constant rate of energy injection).

### 5.1 Results: Interpolation of Models

In Figure 2 (and Figure 3) we see that the physics informed parameterized SPH simulator is learn-able; the estimated physical parameters  $\hat{\alpha}, \hat{\beta}, \hat{c}, \hat{\gamma}$ , and energy injection rate  $\hat{\theta}_{inj}$  converging to the true values where the initial guess for each parameter is uniformly distributed about  $(0, 1)$ . Figure 4 illustrates the ability of the mixed mode method applied to the EoS-NN model to learn (approximate) physically interpretable functions (namely the barotropic equation of state  $P(\rho)$ ) using NNs embedded within an SPH model. However, we notice that the learned EoS  $P_{nn}(\rho)$  begins to deviate from the  $P_{truth}(\rho)$  outside the domain of densities that are seen in training.

In Figure 6, we see that each model is capable of learning the parameters so that the underlying velocity increment distributions are approximated on the time scale on

which learning takes place. Furthermore, In Figure 6 we test the trained models on their ability to reproduce the distribution associated with the single particle dispersion statistic (Yeung & Bogras, 2004) (showing how far the particle disperses from its initial condition on a set time scale). Here it is important to note that the dispersion statistic was not enforced in the  $L_{kl}$  loss, and so Figure 6 illustrates an external diagnostic test. From this we find that without enforcing the dispersion statistic in the loss function, the less informed models (namely NODE, and NN summand) fail to reproduce the true dispersion statistics on both time scales ( $t_\lambda$ , and  $t_{eddy}$ ).

These figures, show that over a mixture of the loss functions  $L_{kl}+L_f$  (subsection 4.4), applying the methods described in subsection 4.2.1, the Lagrangian models (subsection 4.1) are learn-able (interpolated on the SPH training set).

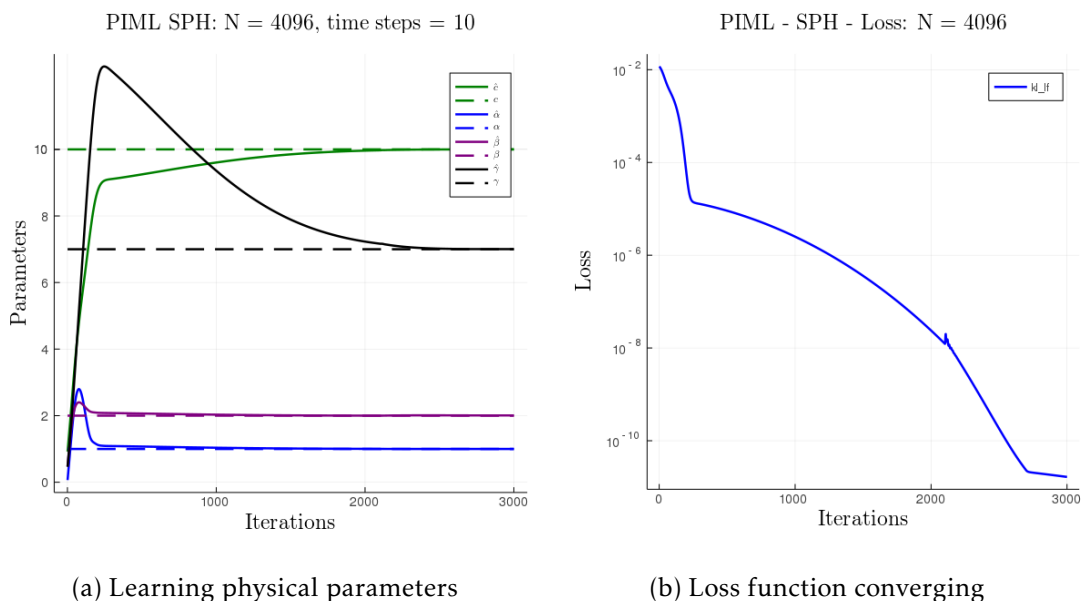


Figure 2: Solving an inverse problem for the fully physics informed model on 3D SPH flow with deterministic external forcing on 4096 particles over the SPH based parameters. The solid lines show the SPH model parameters (initially chosen to be uniformly distributed about (0,1)) converging to the dashed lines representing the ground truth parameters. Here the  $L_{kl} + L_f$  loss function (see subsection 4.4) is used (where  $L_f$  is used in pre-training up to 2100 iterations as seen in the small increase in the loss as the  $L_{kl}$  is added in).

## 5.2 Results: Generalizability (extrapolation capability) on SPH flow data

When the training is complete (i.e. when the loss function reaches its minimum, and conditions are set as described in section 5) we validate extrapolation capability of the models on a validation set, and test data set. The validation data set corresponds to data generated from the same initial conditions but are longer in duration (up to the eddy

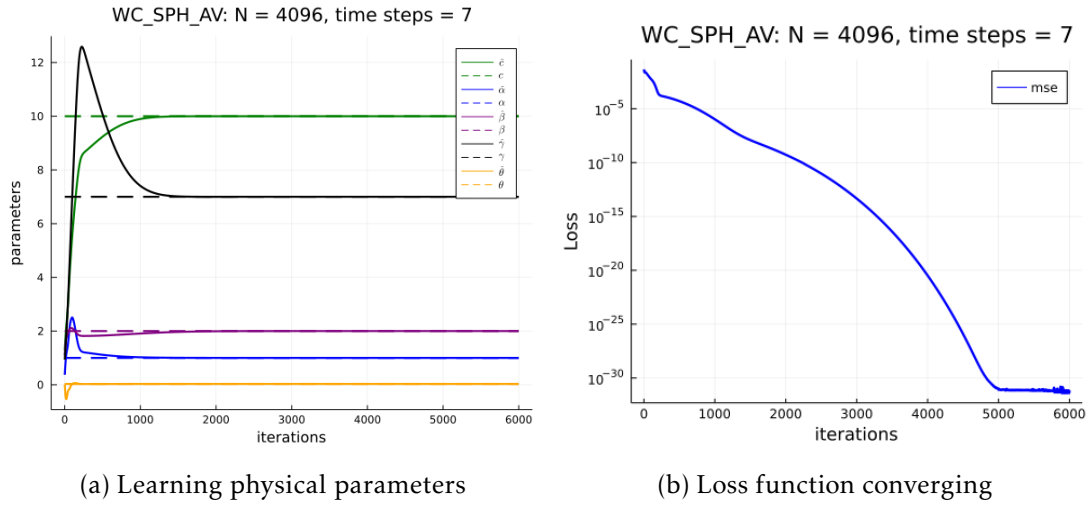


Figure 3: Solving the inverse problems for 3D SPH flow using  $L_f$  with a linear deterministic external forcing on 4096 particles over physical parameters including the rate of energy injection  $\theta_{inj}$ . Notice the field based loss (using MSE) converging to machine precision, validating the learning algorithm

turn over time). The test set corresponds to flow derived from the setting corresponding to stronger turbulent Mach numbers (which we control by increasing intensity of the injection term,  $f_{ext}$ , while keeping the integral, i.e. energy injection scale, constant, thus increasing the turbulent mach number,  $M_t$ ).

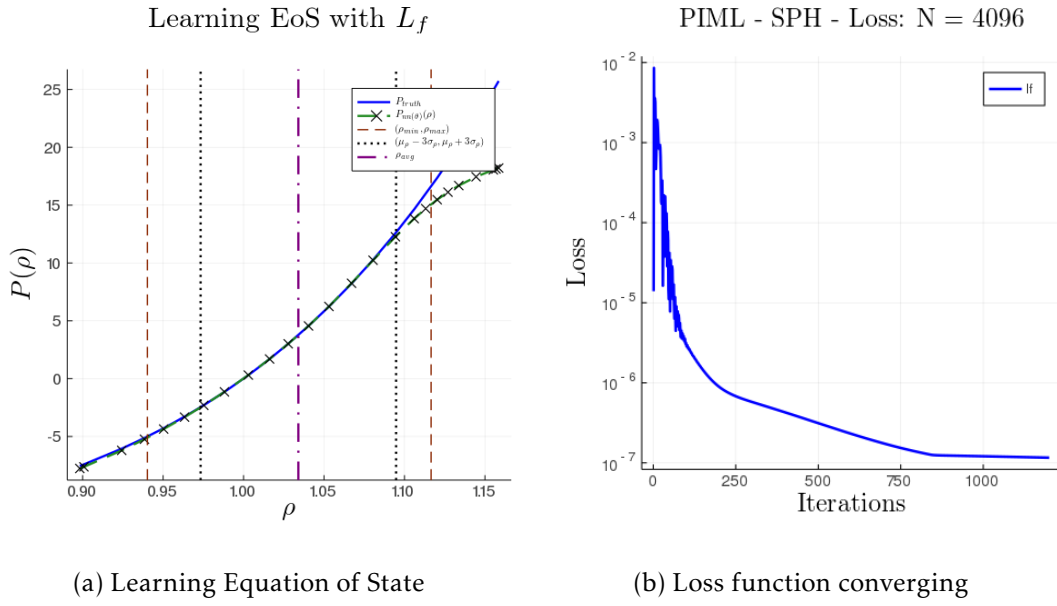


Figure 4: Using a Neural Network to approximate the equation of state (see subsection 4.1) using the field based loss function. We see that  $P(\rho)$  is well approximated, where  $P_{truth}$  is the ground truth EoS and  $P_{nn}$  is the neural network approximation. We note that the underlying ground truth data has 99.73% of density values within the black dotted bars (within 3 standard deviations), and maximum and minimum density values plotted in maroon.

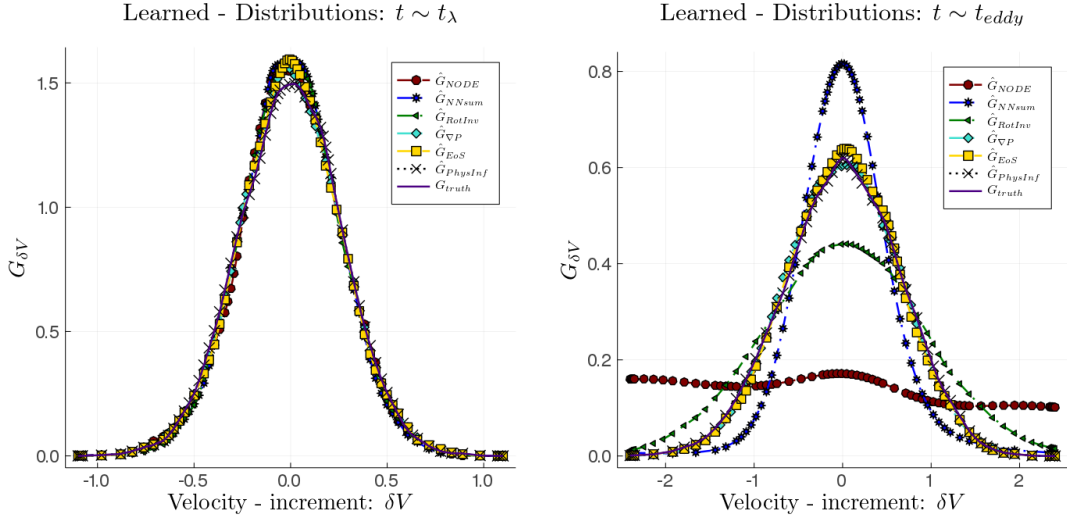


Figure 5: The velocity increment distribution learned over each model in the hierarchy subsection 4.1 on the time scale  $t_\lambda$  using the  $L_{kl} + L_f$  loss function and the FSA method. We see that, on the learned time scale, all the models do well at capturing the small scale Lagrangian velocity increment statistics, however, only the more physics informed models do well at generalizing to larger time scales not seen in training.

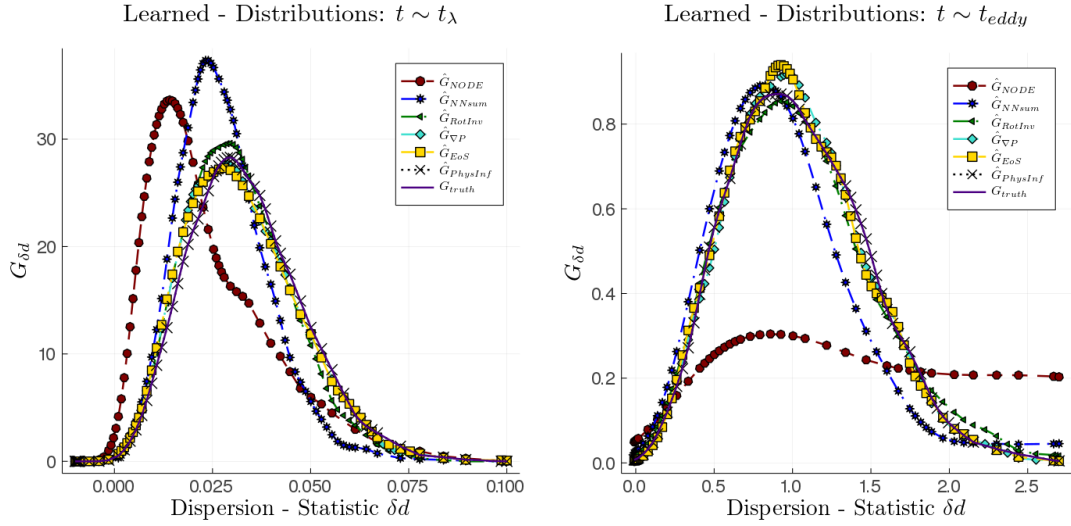


Figure 6: The single particle dispersion statistic distribution being used as a diagnostic check on each model in the hierarchy subsection 4.1 on the learned time scale and on the eddy turn over time scale

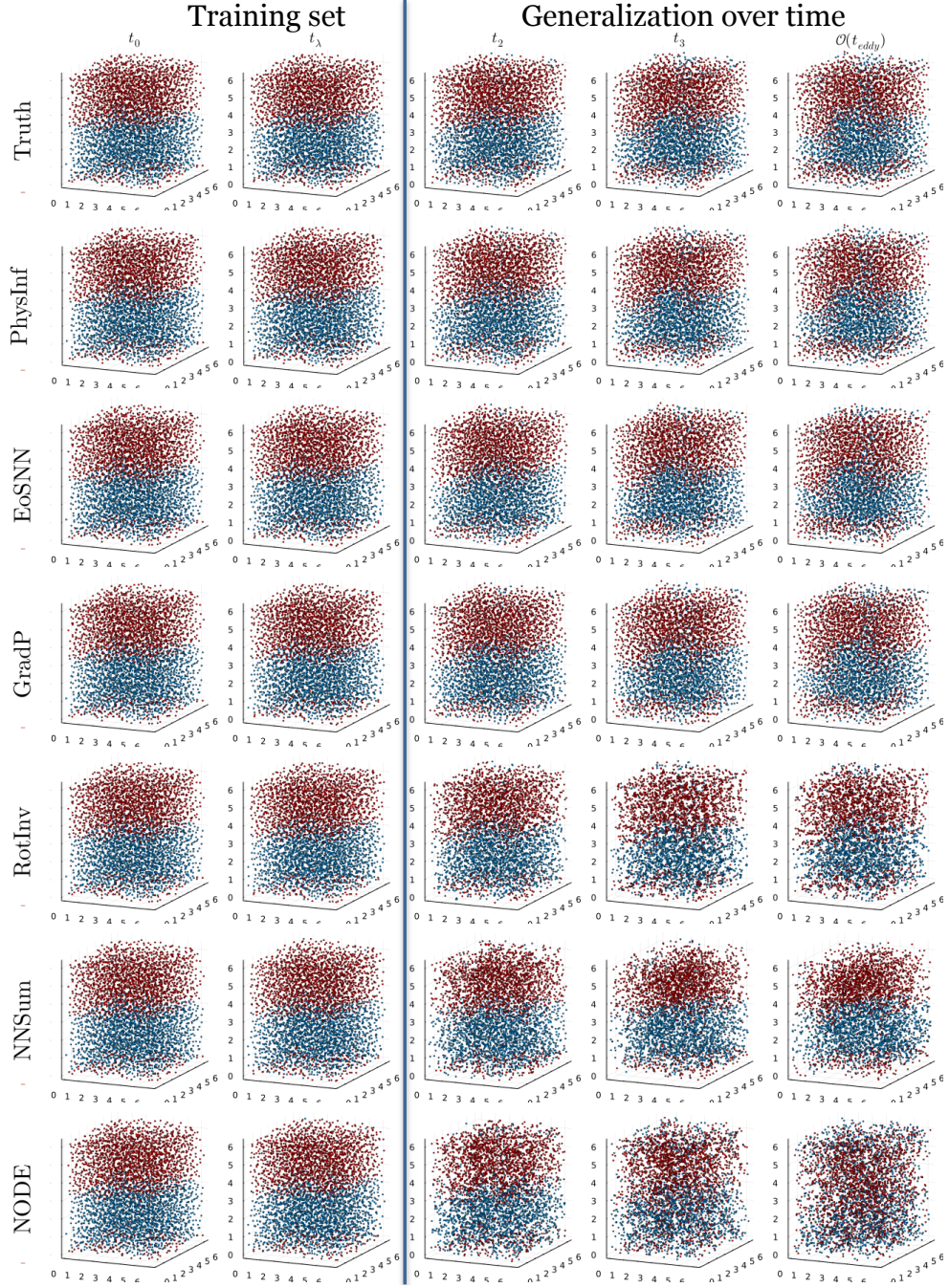
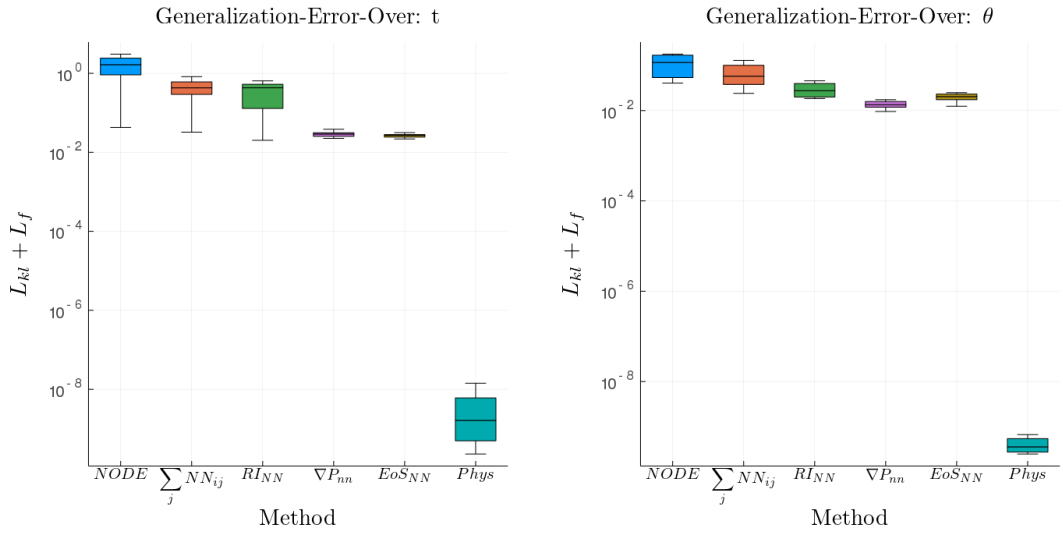


Figure 7: Snapshots of flows comparing the ground truth to the learned models, where learning is done with the  $L_{KL} + L_f$  loss function. Even though the training is occurring on the shortest (physically relevant) time scale  $t_\lambda$  the more physics informed models are able to generalize to much longer time scales – all the way to the longest (physically relevant) time scale,  $t_{eddy}$  (which is the turnover time scale of the largest eddy of the flow).



(a) Generalization error over  $t$

(b) Generalization error over  $M_t$

Figure 8: (a) Box plot using 20 different generalization errors over physically relevant time scales ranging from the shortest,  $t_\lambda$  (which is the time it takes for a pair of initially neighboring particles to double their relative separation), up to the longest,  $t_{eddy}$  (which is the time it takes for the largest eddy of the flow to make a complete revolution). (b) Box plot over 5 different generalization including turbulent Mach numbers  $M_t \in \{0.03, 0.06, 0.08, 0.10, 0.12\}$ , where the time scale is fixed at  $t_\lambda$ .

Table 2: Errors in Rotational and Translational Symmetries on trained models

Trained Model	Rotational Error	Translational Error
NODE	4.59	6.57
NN Sum	5.42	1.51
Rot Inv	$1.21 \times 10^{-27}$	$4.22 \times 10^{-27}$
$\nabla P$	$1.20 \times 10^{-2}$	$1.48 \times 10^{-27}$
EoS NN	$3.49 \times 10^{-28}$	$1.18 \times 10^{-27}$
Phys Inf	$2.31 \times 10^{-27}$	$7.88 \times 10^{-27}$

We observe in Figure 8, showing results for trained models using  $L_f + L_{kl}$ , that the richer (physical) SPH structure added to the model is, the lower the generalization error becomes when we extrapolate to flows with larger  $M_t$  numbers and over different time scales. This is to be expected for training SPH informed models on SPH data, however, we will see a similar trend in section 6 when we train on Eulerian DNS data. Furthermore, Table 2 shows that as more SPH structure is added to the model, the error in rotational and translational invariance (see Appendix C) of the learned acceleration operator decreases (and therefore conservation of angular and linear momentum is preserved). Additional qualitative generalizability results in Figure 7, along with the interpolation results above, demonstrates that data (samples of particle trajectories) of much shorter (temporal) duration are required to train models which are more physics informed (where a short time duration,  $t_\lambda$ , is used in training, and we see the converged models extrapolating to longer time scales not seen in training). Figure 7 also shows, qualitatively, that the large scales structures of the flows are well preserved as we extrapolate for longer times than used in training.

## 6 Results: Evaluating and Testing Models on DNS data

In this section we illustrate and analyze the hierarchy of models trained on weakly compressible (low Mach number) Eulerian based DNS data. We explore similar diagnostics to the above section, and demonstrate generalizability to different time scales and turbulent Mach numbers  $M_t \in \{0.04, 0.08, 0.16\}$ . Each model is trained using the field based loss with  $M_t = 0.08$  and over the Kolmogorov time scale (roughly  $1.2(s)$  or 60 time steps). When generalizing to larger time scales (with the same  $M_t$ ) the trained models are integrated up to the eddy turn over time and compared with the DNS data. When testing generalizability of each model to different turbulent Mach numbers, the learned model parameters are fixed and the models are integrated up to the Kolmogorov time with the energy injection rate parameter scaled proportionally (with constant ratio over each model) in order to match the turbulent Mach number in the DNS data.

## 6.1 DNS data

In this work, the “ground-truth” (GT) Lagrangian data is generated from the Eulerian Direct Numerical Simulation (DNS) of the compressible Navier-Stokes (NS) equations. The compressible Navier-Stokes equations with low turbulent Mach number ( $M_t$ ) is compatible with the weakly compressible SPH formulation. In this work, we numerically solve the dimensionless compressible NS equation on a  $256^3$  mesh with sixth-order compact scheme for spatial discretization and 4th-order Runge-Kutta scheme for time advancement. The computational domain is  $(2\pi, 2\pi, 2\pi)$  and triply-periodic boundary condition is used. The velocity field for the isotropic turbulence is initialized randomly following a 3D Gaussian spectral density function with the average velocity being zero. A large-scale linear forcing term is applied to the simulation at wavenumber  $|k| < 4$  to prevent the turbulence from decaying (Petersen & Livescu, 2010). The initial temperature field is set to be uniform and the initial pressure field is calculated by solving the Poisson equation. The simulation is conducted until the turbulence becomes fully-developed, which can be verified when the skewness and flatness of the velocity derivatives reach  $-0.5$  and  $4.0$ .

After the turbulence reaches a statistically-steady state, a total number of  $16^3$  non-inertial Lagrangian fluid particles are initially configured on a lattice in the computational domain. The evolution of the non-inertial Lagrangian particles is computed by integrating  $\dot{\mathbf{x}} = \mathbf{v}$ , where the velocity on the right-hand side (RHS) is the filtered Eulerian velocity from DNS simulations. In this study, we use a Gaussian filter, which is commonly used in LES, with a filtering length scale  $l_\delta$  that can be resolved by the number of SPH particles used in the simulation.

## 6.2 Comparing Smoothing Kernels

In Figure 9 we compare three different smoothing kernels; two standard and fixed smoothing kernels, namely the cubic Eq. (16) and quartic Eq. (17) splines (which follow the Gaussian bell shape); and a novel parameterized smoothing kernel that is learned from DNS data when training Eq. (11). In the following subsections we show that including this novel parameterized smoothing kernel in training improves the ability of the SPH informed model to solve the interpolation problem and generalize to flows not seen in training. This result seems to suggest that an improvement to the SPH construction can be made, at least in the weakly compressible setting at the resolved scales as seen in this work, by considering smoothing kernels which are not of the classical bell shape, but rather of the more flexible and parameterized form proposed in Eq. (12). Future work could be done in this direction to further analyze and compare this new smoothing kernel with regards to convergence and consistency.

## 6.3 Comparing Equations of State

In the trained SPH informed models Eq. (9), Eq. (10), and Eq. (11), parameterized barotropic Equations of State (EoS) are learned. In the EoS NN model, a neural net-

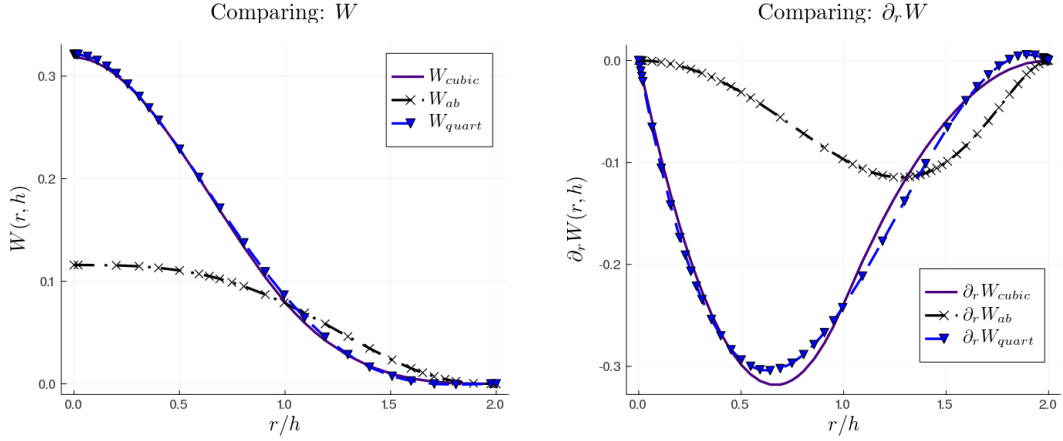


Figure 9: Comparing learned smoothing kernel  $W(r; h, a, b)$  with standard cubic Eq. (16) and quartic Eq. (17) kernels. Notice the shape of the learned parameterized smoothing kernel includes a relatively larger contribution from particles farther away

work is used to approximate the EoS, whereas in the Fully Physics Informed models, the EoS is modeled by the parameterized equation  $P(\rho) = c^2 \rho^\gamma + p_0$  where  $c$ ,  $\gamma$ , and  $p_0$  are learned. Note that the background pressure  $p_0$  is known to change the dynamics when the pressure gradient term is approximated by the symmetrized form ( see Eq. (19)), and including this as a learn-able parameter is found to improve the fit and generalizability. From Figure 11 and Table 3, we see that the equation of state modeled by the NN performs best at capturing the underlying ground truth speed of sound.

Table 3: Comparing learned values of speed of sound

Model	Speed of sound (c)
DNS Ground truth	1.00
Eq. (9) EoS NN ( $P_{nn}$ )	1.02
Eq. (11) $W_{ab}$	0.94
Eq. (10) $W_{cub}$	0.78

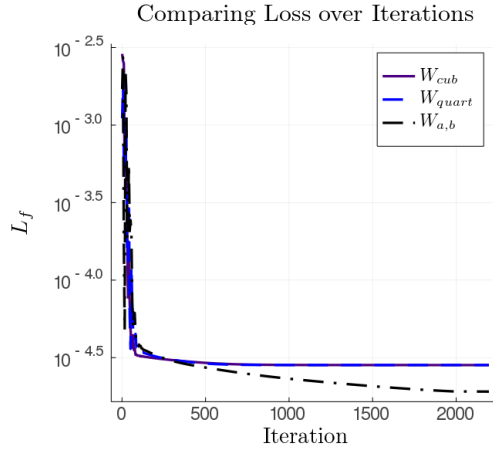


Figure 10: Convergence of loss, comparing the effects of using different smoothing kernels training on DNS data using  $L_f$ . The parameterized smoothing kernel based model converges to a lower value.

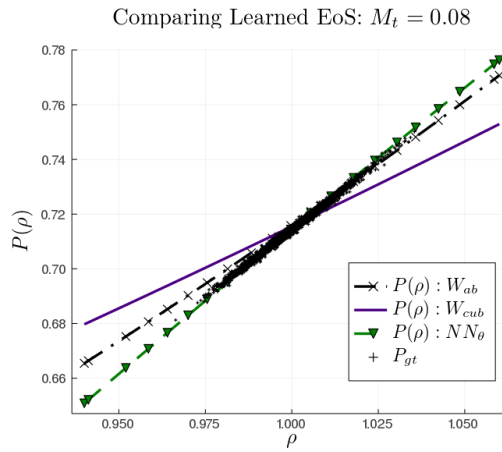


Figure 11: Comparing the learned equations of state.  $P(\rho) : W_{ab}$  comes from Eq. (11),  $P(\rho) : W_{cub}$  Eq. (10), and  $P(\rho) : NN_\theta$  from Eq. (9)

## 6.4 Generalizability

In this subsection, we compare each learned parameterized model in their ability to generalize to longer time scales and different turbulent Mach numbers. Overall, we find the trend that as more SPH structure is included in the model, the better is its ability to generalize, with Eq. (11) (which includes the parameterized smoothing kernel) performing the best. Both quantitative and qualitative measures of performance are used. We use the field based loss as a quantitative measure Figure 13 comparing each model over larger time scales and different turbulent Mach numbers. The error in translational and rotational symmetries are compared in Figure 14 which shows that as more SPH based structure is included, conservation of linear and angular momenta are enforced. We use several qualitative measures such as the energy spectrum Figure 16, acceleration pdf Figure 18, and single particle statistics Figure 15 to evaluate the statistical performance of each model. From which, we can conclude that the physics informed model including the novel parameterized smoothing kernel (Eq. (11)) performs best at generalizing with respect to the quantitative and qualitative performance evaluations to larger time scales and different turbulent Mach numbers.

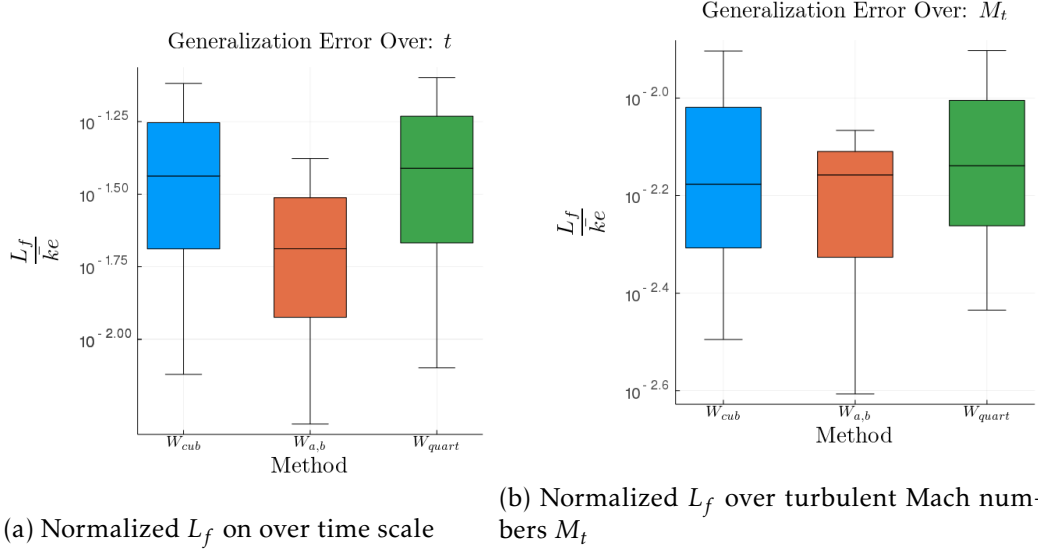


Figure 12: Comparing SPH informed models with three different smoothing kernels (cubic and quartic spline and parameterized smoothing kernel denoted  $W_{ab}$  Eq. (12)). Measuring the relative error of  $L_f$  as a percentage of total kinetic energy over three different turbulent Mach numbers  $\{0.04, 0.08, 0.16\}$ .

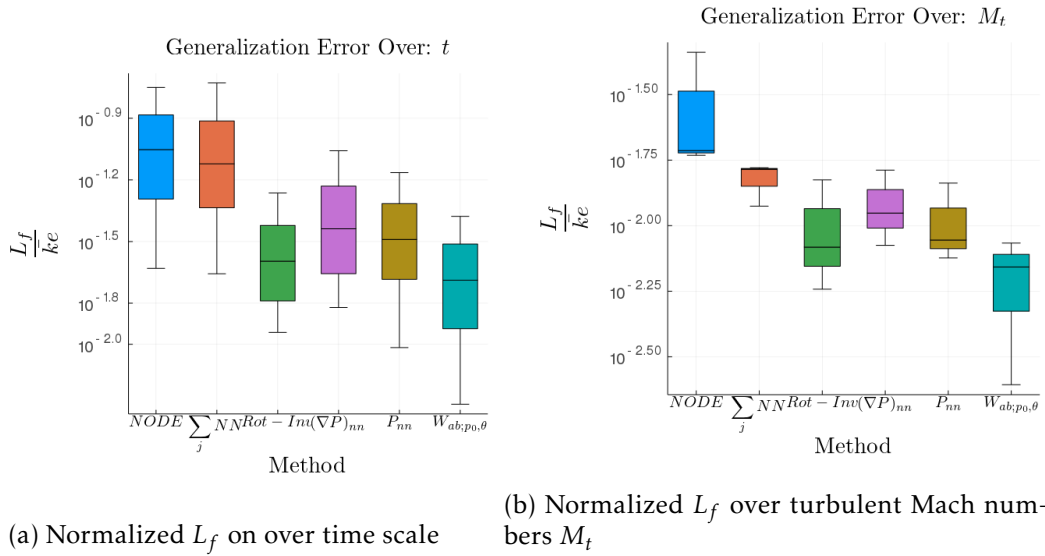


Figure 13: Measuring the relative error of  $L_f$  as a percentage of total kinetic energy. The generalization error over  $M_t$  is computed over 3 different turbulent Mach numbers  $M_t \in \{0.04, 0.08, 0.16\}$ . We see that the parameterized smoothing kernel model and rotationally invariant NN based model performs best under this field based measure.

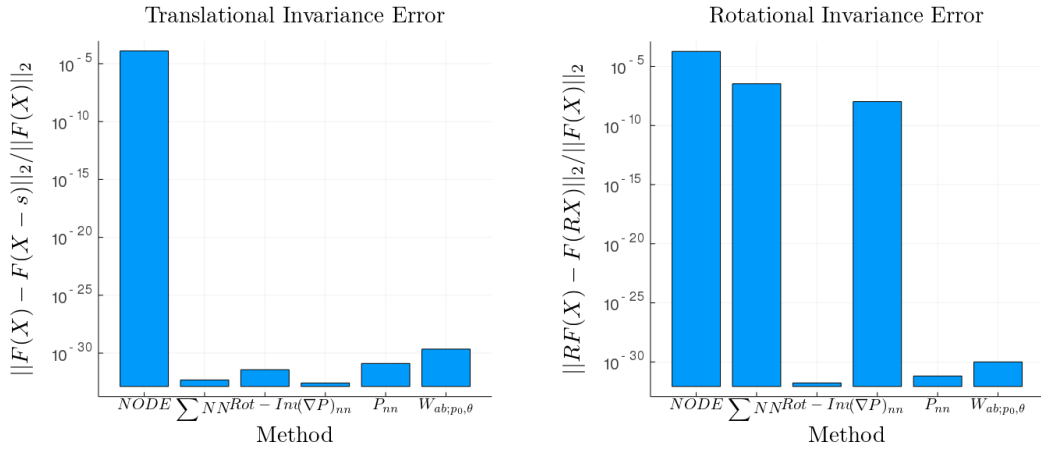


Figure 14: Errors in normalized translational and rotational invariance of each trained model using DNS data with  $M_t = 0.16$ .

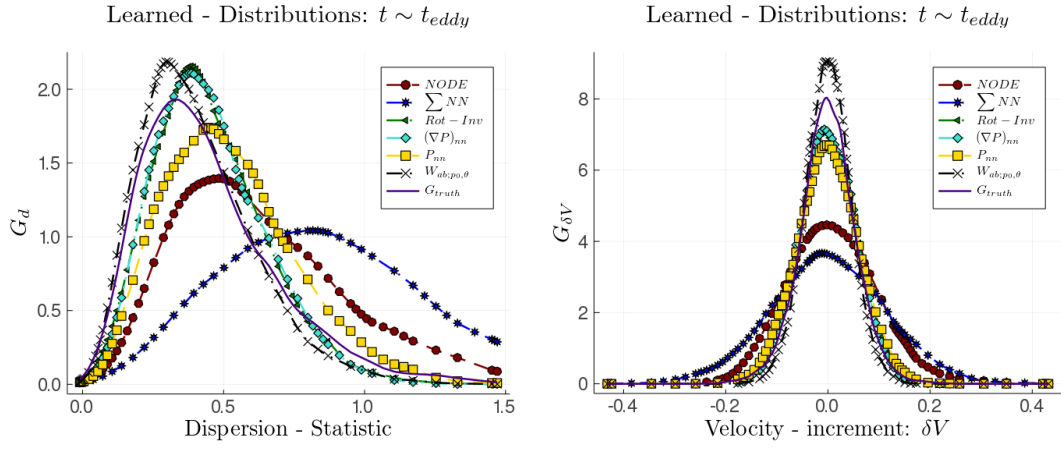


Figure 15: A diagnostic check comparing single particle statistics on larger time scales (roughly 8 times longer than seen in training), with the new parameterized smoothing kernel based SPH model having the best fit

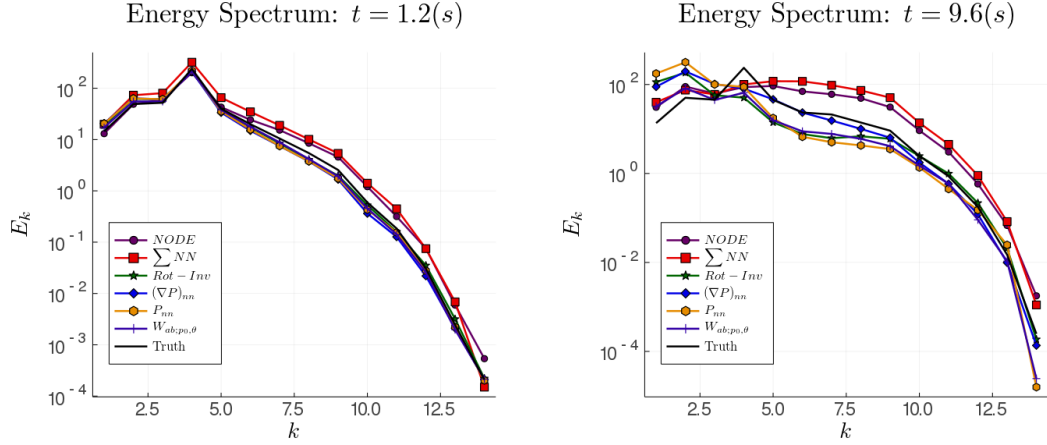


Figure 16: Comparing energy spectrum over time;  $t = 1.2s$  is on the Kolmogorov time scale, where  $t_{eddy} \approx 9.6s$ . We see that the more physics informed models do a better job a reproducing the energy cascade seen in DNS on both the training time scale and in generalizing to larger time scales

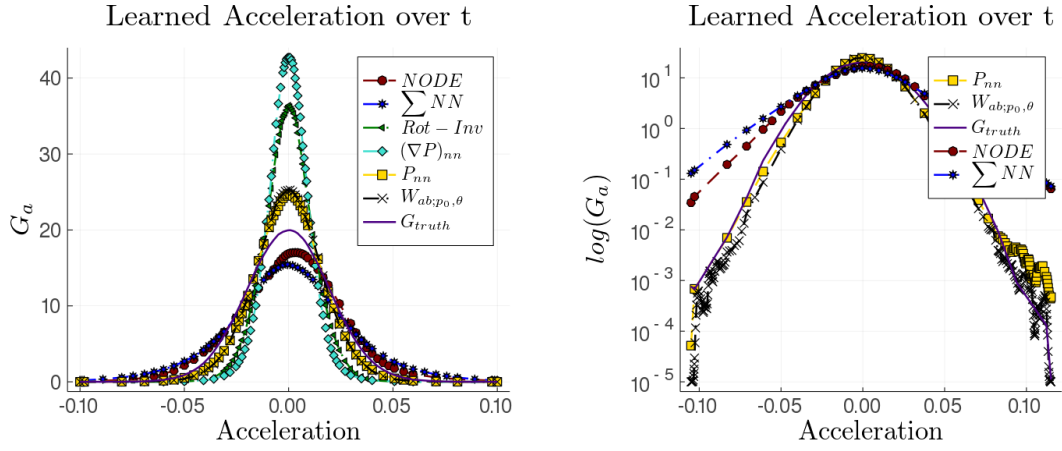


Figure 17: Acceleration pdf over longer time scales (combined) seen in training. The new parameterized smoothing kernel and EoS NN model are seen to have the best generalization over longer time scales. The acceleration pdf is used as an external qualitative diagnostic (not used in training), and demonstrates the abilities of the models to learn the true acceleration operator.

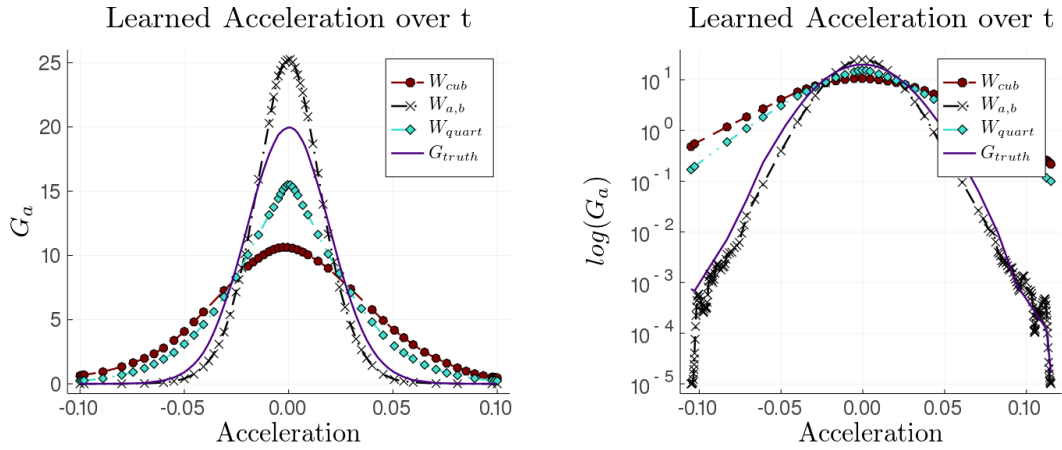


Figure 18: Acceleration pdf over longer time scales (combined) seen in training comparing the effects of using different smoothing kernels. This shows the ability of the new parameterized smoothing kernel to better generalize in capturing the true acceleration operator over longer time scales.

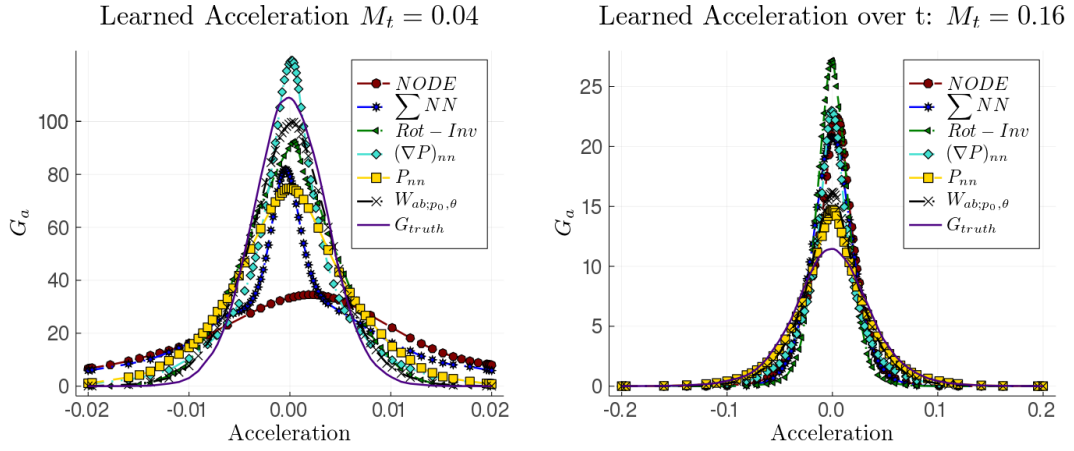


Figure 19: Acceleration pdf as another external diagnostic check over different turbulent Mach numbers. The new parameterized smoothing kernel and EoS NN model are seen to have the best generalization over different turbulent Mach numbers, especially to larger  $M_t$ .

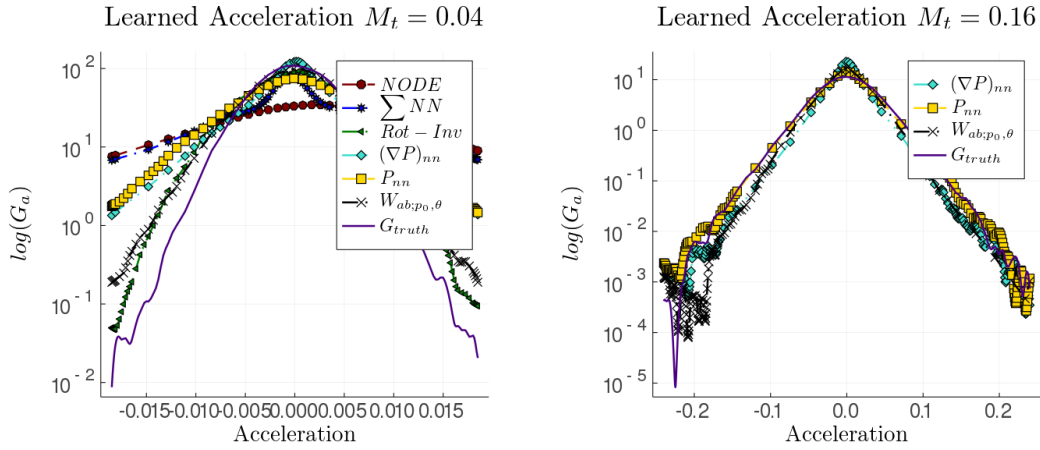


Figure 20: Log plot of Figure 19

## 7 Conclusions

Combining SPH based modeling, deep learning, automatic differentiation, and local sensitivity analysis, we have developed a learn-able hierarchy of parameterized "physics-explainable" Lagrangian fluid simulators, and compared each trained model on both weakly compressible SPH and DNS data.

Starting from a Neural ODE based model, we showed that incrementally adding more physical structure into the Lagrangian models (on both "clean" SPH data and "real world" DNS data) has several important benefits:

- Improves generalizability. This can be seen in subsection 5.2 and subsection 6.4, where we test the ability of the models to predict flows under different conditions not seen in training. The general trend emerged: as more physics informed SPH based structure is embedded in the model, the lower the generalization error became.
- Learning new smoothing kernels subsection 6.2. A key ingredient in the construction of the SPH method relies on the properties of the smoothing kernel. A novel parameterized and learn-able smoothing kernel is developed which increases the flexibility of the physics informed SPH based models and improved the generalizability on DNS data compared to standard smoothing kernels.
- Improves reconstruction of the hidden physical relations. For example, as more of the physical structure is embedded into the SPH based models, the better its ability to conserve linear and angular momenta, associated with translational and rotational symmetries, respectively. This can be seen in Table 2, and Figure 14.
- Improves overall interpretability, as the learned parameters become physically meaningful (as opposed to NN parameters, although each NN in the hierarchy is approximating an interpretable function). For example, in the fully physics informed model (as seen in subsection 4.1), the learned (estimated) parameters directly correspond to physically interpretable quantities such as the equation of state, artificial shear and bulk viscosity, and external forcing.
- Requires less training data Figure 7, and is more efficient to train Table 1 compared to less informed models (such as Neural ODE).

### 7.1 Future work

We plan to go beyond the SPH-based inverse Lagrangian modeling discussed so far. Specifically, we aim to build Reduced-Order Lagrangian Models of Turbulence based on the SPH method and validate it against realistic turbulence data originated from direct numerical simulations and/or experiments. Our goal is to develop the PIML based Lagrangian SPH approach to the degree that it allows the discovery of reduced turbulence models which are capable in extrapolating into difficult regimes, e.g. of larger  $Re$  number and stronger degree of compressibility, where the data are limited.

## 8 Reproducibility Statement

Supplementary material <https://github.com/mwoodward-cpu/LearningSPH> includes the Julia source code of our parameterized SPH simulators, the gradient based learning algorithm, and sensitivity calculations for each model in the above hierarchy. The general steps to take in order to reproduce these results are as follows: generate SPH ground truth flows using the parameters described in section 3 (or using DNS data provided), then use this data for learning the hierarchy of models found in the `main_*.jl` files; which requires a selection of the model, loss function, sensitivity method, number of iterations, and height. Note, with the heights proposed in subsection 4.1, most of the models containing NNs have a total number of parameters on the order  $p \sim \mathcal{O}(100)$ ; in this case FSA is more efficient. The trained models are provided in the output data files which are used in post-processing (all found in the github repository).

### Acknowledgments

*This work was supported by DOE funding via LANL/LDRD/DR project on “MELT: Machine Learning for Turbulence”.*

*This material is based upon work supported by the U.S. Department of Energy, Office of Science, Office of Workforce Development for Teachers and Scientists, Office of Science Graduate Student Research (SCGSR) program. The SCGSR program is administered by the Oak Ridge Institute for Science and Education (ORISE) for the DOE. ORISE is managed by ORAU under contract number DE-SC0014664. All opinions expressed in this paper are the author’s and do not necessarily reflect the policies and views of DOE, ORAU, or ORISE.*

### References

- Jeff Bezanson, Alan Edelman, Stefan Karpinski, and Viral B Shah. Julia: A fresh approach to numerical computing. *SIAM review*, 59(1):65–98, 2017. URL <https://doi.org/10.1137/141000671>.
- Andrew Bradley. PDE Constrained Optimization and the Adjoint Method. [cs.stanford.edu](https://cs.stanford.edu), 2019. URL [https://cs.stanford.edu/~ambrad/adjoint\\_tutorial.pdf](https://cs.stanford.edu/~ambrad/adjoint_tutorial.pdf).
- Martin Bücker. *Automatic Differentiation Applications, Theory and Implementations*. Springer, 2006.
- Shengze Cai, Jiaming Liang, Qi Gao, Chao Xu, and Runjie Wei. Particle image velocimetry based on a deep learning motion estimator. *IEEE Transactions on Instrumentation and Measurement*, 2019.
- Ricky T. Q. Chen, Yulia Rubanova, Jesse Bettencourt, and David Duvenaud. Neural ordinary differential equations. [arXiv:1806.07366](https://arxiv.org/abs/1806.07366), 2019.

Yen-Chi Chen. A tutorial on kernel density estimation and recent advances. Biostatistics & Epidemiology, 1(1):161–187, 2017. doi: 10.1080/24709360.2017.1396742. URL <https://doi.org/10.1080/24709360.2017.1396742>.

CNLS at LANL. Physics Informed Machine Learning (PIML) workshop. <http://www.cvent.com/events/3rd-physics-informed-machine-learning/event-summary-f98f02016,2018,2020>.

Peter J. Cossins. Smoothed particle hydrodynamics. arXiv:1007.1245, 2010.

Juan de Anda-Suárez, Martín Carpio, Solai Jeyakumar, Héctor Soberanes, Juan Mosiño, and Laura Cruz Reyes. Optimization of the Parameters of Smoothed Particle Hydrodynamics Method, Using Evolutionary Algorithms. pp. 153–167. Springer, 01 2018. ISBN 978-3-319-71007-5. doi: 10.1007/978-3-319-71008-2\_13.

Li Deng and Yang Liu. Deep Learning in Natural Language Processing. Springer, 2018.

J. M. Domínguez, A. J. C. Crespo, M. Gómez-Gesteira, and J. C. Marongiu. Neighbour lists in smoothed particle hydrodynamics. International Journal for Numerical Methods in Fluids, 67(12):2026–2042, 2011. doi: <https://doi.org/10.1002/flid.2481>. URL <https://onlinelibrary.wiley.com/doi/abs/10.1002/flid.2481>.

Michael Donello, Mark Carpenter, and Hessam Babae. Computing sensitivities in evolutionary systems: A real-time reduced order modeling strategy. arXiv:2012.14028, 2020.

Karthik Duraisamy, Gianluca Iaccarino, and Heng Xiao. Turbulence modeling in the age of data. Annual Review of Fluid Mechanics, 51(1):357–377, 2019. doi: 10.1146/annurev-fluid-010518-040547. URL <https://doi.org/10.1146/annurev-fluid-010518-040547>.

Enrico Fonda, Amrish Pandey, Jörg Schumacher, and Katepalli R. Sreenivasan. Deep learning in turbulent convection networks. Proceedings of the National Academy of Sciences, 116(18):8667–8672, 2019. ISSN 0027-8424. doi: 10.1073/pnas.1900358116. URL <https://www.pnas.org/content/116/18/8667>.

U. Frisch. Turbulence: The Legacy of AN Kolmogorov. Cambridge University Press, 1995.

David A. Fulk and Dennis W. Quinn. An analysis of 1-d smoothed particle hydrodynamics kernels. Journal of Computational Physics, 126(1):165–180, 1996. ISSN 0021-9991. doi: <https://doi.org/10.1006/jcph.1996.0128>. URL <https://www.sciencedirect.com/science/article/pii/S002199919690128X>.

R. A. Gingold and J. J. Monaghan. Smoothed particle hydrodynamics: theory and application to non-spherical stars. Monthly Notices of the Royal Astronomical Society, 181:375–389, Nov 1977.

- Francis H. Harlow. Fluid dynamics in Group T-3 Los Alamos National Laboratory: (LA-UR-03-3852). Journal of Computational Physics, 195(2):414–433, 2004. ISSN 0021-9991. doi: <https://doi.org/10.1016/j.jcp.2003.09.031>. URL <https://www.sciencedirect.com/science/article/pii/S0021999103005692>.
- Kurt Hornik, Maxwell Stinchcombe, and Halbert White. Multilayer feedforward networks are universal approximators. Neural Networks, 2(5):359–366, 1989. ISSN 0893-6080. doi: [https://doi.org/10.1016/0893-6080\(89\)90020-8](https://doi.org/10.1016/0893-6080(89)90020-8). URL <https://www.sciencedirect.com/science/article/pii/0893608089900208>.
- Michael Innes. Don't unroll adjoint: Differentiating ssa-form programs. CoRR, abs/1810.07951, 2018. URL <http://arxiv.org/abs/1810.07951>.
- Michael Innes, Elliot Saba, Keno Fischer, Dhairya Gandhi, Marco Concetto Rudilosso, Neethu Mariya Joy, Tejan Karmali, Avik Pal, and Viral Shah. Fashionable modelling with flux. CoRR, abs/1811.01457, 2018. URL <https://arxiv.org/abs/1811.01457>.
- Ryan King, Oliver Hennigh, Arvind Mohan, and Michael Chertkov. From Deep to Physics-Informed Learning of Turbulence: Diagnostics. arXiv:1810.07785, 2018.
- Diederik P. Kingma and Jimmy Ba. Adam: A method for stochastic optimization. 2017.
- Robert H. Kraichnan. Kolmogorov's hypotheses and eulerian turbulence theory. The Physics of Fluids, 7(11):1723–1734, 1964. doi: 10.1063/1.2746572. URL <https://aip.scitation.org/doi/abs/10.1063/1.2746572>.
- Robert H. Kraichnan. Lagrangian-history closure approximation for turbulence. The Physics of Fluids, 8(4):575–598, 1965. doi: 10.1063/1.1761271. URL <https://aip.scitation.org/doi/abs/10.1063/1.1761271>.
- L'ubor Ladický, SoHyeon Jeong, Barbara Solenthaler, Marc Pollefeys, and Markus Gross. Data-Driven Fluid Simulations Using Regression Forests. ACM Trans. Graph., 34(6), October 2015. ISSN 0730-0301. doi: 10.1145/2816795.2818129. URL <https://doi.org/10.1145/2816795.2818129>.
- I.E. Lagaris, A. Likas, and D.I. Fotiadis. Artificial neural networks for solving ordinary and partial differential equations. IEEE Transactions on Neural Networks, 9(5):987–1000, 1998. ISSN 1045-9227. doi: 10.1109/72.712178. URL <http://dx.doi.org/10.1109/72.712178>.
- Yong Lee, Hua Yang, and Zhouping Yin. Piv-dcnn: cascaded deep convolutional neural networks for particle image velocimetry. Experiments in Fluids, 58(12):171, 2017.
- Steven J. Lind, Benedict D. Rogers, and Peter K. Stansby. Review of smoothed particle hydrodynamics: towards converged lagrangian flow modelling. Proceedings of the Royal Society A: Mathematical, Physical and Engineering Sciences, 476(2241):20190801, 2020. doi: 10.1098/rspa.2019.0801. URL <https://royalsocietypublishing.org/doi/abs/10.1098/rspa.2019.0801>.

- Julia Ling, Andrew Kurzawski, and Jeremy Templeton. Reynolds averaged turbulence modelling using deep neural networks with embedded invariance. Journal of Fluid Mechanics, 807:155–166, 2016. doi: 10.1017/jfm.2016.615.
- M. B. Liu and G. R. Liu. Smoothed Particle Hydrodynamics (SPH): an Overview and Recent Developments. Archives of Computational Methods in Engineering, 17:25–76, 2010a.
- M. B. Liu and G. R. Liu. Smoothed Particle Hydrodynamics (SPH): an Overview and Recent Developments. Archives of Computational Methods in Engineering, 17(1): 25–76, 2010b. doi: 10.1007/s11831-010-9040-7. URL <https://doi.org/10.1007/s11831-010-9040-7>.
- L. B. Lucy. A numerical approach to the testing of the fission hypothesis. Astronomical Journal, 82:1013–1024, December 1977. doi: 10.1086/112164.
- Yingbo Ma, Vaibhav Dixit, Mike Innes, Xingjian Guo, and Christopher Rackauckas. A comparison of automatic differentiation and continuous sensitivity analysis for derivatives of differential equation solutions. arXiv:1812.01892, 2021.
- Romit Maulik, Arvind Mohan, Bethany Lusch, Sandeep Madireddy, Prasanna Balaprakash, and Daniel Livescu. Time-series learning of latent-space dynamics for reduced-order model closure. Physica D: Nonlinear Phenomena, 405:132368, Apr 2020. ISSN 0167-2789. doi: 10.1016/j.physd.2020.132368. URL <http://dx.doi.org/10.1016/j.physd.2020.132368>.
- Arvind T. Mohan and Datta V. Gaitonde. A deep learning based approach to reduced order modeling for turbulent flow control using lstm neural networks. <https://arxiv.org/abs/1911.05180v1>, 2018.
- Arvind T. Mohan, Nicholas Lubbers, Daniel Livescu, and Michael Chertkov. Embedding hard physical constraints in neural network coarse-graining of 3d turbulence. arXiv:2002.00021, 2020a.
- Arvind T. Mohan, Dima Tretiak, Misha Chertkov, and Daniel Livescu. Spatio-temporal deep learning models of 3d turbulence with physics informed diagnostics. Journal of Turbulence, 21(9-10):484–524, 2020b. doi: 10.1080/14685248.2020.1832230. URL <https://doi.org/10.1080/14685248.2020.1832230>.
- J. J. Monaghan. Smoothed particle hydrodynamics. Annual Review of Astronomy and Astrophysics, 30(1):543–574, 1992. doi: 10.1146/annurev.aa.30.090192.002551. URL <https://doi.org/10.1146/annurev.aa.30.090192.002551>.
- J. J. Monaghan. Smoothed particle hydrodynamics. Reports on Progress in Physics, 68(8):1703–1759, Aug 2005.

- J.J. Monaghan. SPH and Riemann Solvers. Journal of Computational Physics, 136(2): 298–307, 1997. ISSN 0021-9991. doi: <https://doi.org/10.1006/jcph.1997.5732>. URL <https://www.sciencedirect.com/science/article/pii/S0021999197957326>.
- J.J. Monaghan. Smoothed particle hydrodynamics and its diverse applications. Annual Review of Fluid Mechanics, 44(1):323–346, 2012. doi: 10.1146/annurev-fluid-120710-101220. URL <https://doi.org/10.1146/annurev-fluid-120710-101220>.
- J.J. Monaghan and R.A. Gingold. Shock simulation by the particle method SPH. Journal of Computational Physics, 52(2):374–389, 1983. ISSN 0021-9991. doi: [https://doi.org/10.1016/0021-9991\(83\)90036-0](https://doi.org/10.1016/0021-9991(83)90036-0). URL <https://www.sciencedirect.com/science/article/pii/0021999183900360>.
- Joseph P. Morris, Patrick J. Fox, and Yi Zhu. Modeling Low Reynolds Number Incompressible Flows Using SPH. Journal of Computational Physics, 136(1):214–226, 1997. ISSN 0021-9991. doi: <https://doi.org/10.1006/jcph.1997.5776>. URL <https://www.sciencedirect.com/science/article/pii/S0021999197957764>.
- A. G. Nouri, H. Babaei, P. Givi, H. K. Chelliah, and D. Livescu. Skeletal model reduction with forced optimally time dependent modes. Combustion and Flame, 235:111684, 2022. doi: <https://doi.org/10.1016/j.combustflame.2021.111684>. URL <https://doi.org/10.1016/j.combustflame.2021.111684>.
- Mark R. Petersen and Daniel Livescu. Forcing for statistically stationary compressible isotropic turbulence. Physics of Fluids, 22(11):116101, 2010. doi: 10.1063/1.3488793. URL <https://doi.org/10.1063/1.3488793>.
- Jean Rabault, Jostein Kolaas, and Atle Jensen. Performing particle image velocimetry using artificial neural networks: a proof-of-concept. Measurement Science and Technology, 28(12):125301, 2017.
- Christopher Rackauckas, Yingbo Ma, Julius Martensen, Collin Warner, Kirill Zubov, Rohit Supekar, Dominic Skinner, Ali Ramadhan, and Alan Edelman. Universal differential equations for scientific machine learning. <https://arxiv.org/abs/2001.04385>, 2020.
- Maziar Raissi, Paris Perdikaris, and George Em Karniadakis. Physics informed deep learning (part ii): Data-driven discovery of nonlinear partial differential equations. arXiv:1711.10566, 2017.
- J. Revels, M. Lubin, and T. Papamarkou. Forward-mode automatic differentiation in Julia. arXiv:1607.07892 [cs.MS], 2016. URL <https://arxiv.org/abs/1607.07892>.
- Connor Schenck and Dieter Fox. Spnets: Differentiable fluid dynamics for deep neural networks. In Aude Billard, Anca Dragan, Jan Peters, and Jun Morimoto (eds.), Proceedings of The 2nd Conference on Robot Learning, volume 87 of Proceedings

- of *Machine Learning Research*, pp. 317–335. PMLR, 29–31 Oct 2018. URL <http://proceedings.mlr.press/v87/schenck18a.html>.
- Thomas Serre. Deep learning: The good, the bad, and the ugly. *Annual Review of Vision Science*, 5(1):399–426, 2019. doi: 10.1146/annurev-vision-091718-014951. URL <https://doi.org/10.1146/annurev-vision-091718-014951>. PMID: 31394043.
- M.S. Shadloo, G. Oger, and D. Le Touzé. Smoothed particle hydrodynamics method for fluid flows, towards industrial applications: Motivations, current state, and challenges. *Computers & Fluids*, 136:11–34, 2016. ISSN 0045-7930. doi: <https://doi.org/10.1016/j.compfluid.2016.05.029>. URL <https://www.sciencedirect.com/science/article/pii/S0045793016301773>.
- Nikolay Stulov and Michael Chertkov. Neural particle image velocimetry. [arXiv:2101.11950](https://arxiv.org/abs/2101.11950), 2021.
- Yifeng Tian, Daniel Livescu, and Michael Chertkov. Physics-informed machine learning of the lagrangian dynamics of velocity gradient tensor. *Phys. Rev. Fluids*, 6: 094607, Sep 2021. doi: 10.1103/PhysRevFluids.6.094607. URL <https://link.aps.org/doi/10.1103/PhysRevFluids.6.094607>.
- Benjamin Ummenhofer, Lukas Prantl, Nils Thuerey, and Vladlen Koltun. Lagrangian Fluid Simulation with Continuous Convolutions. In *International Conference on Learning Representations*, 2020.
- Yasi Wang, Hongxun Yao, and Sicheng Zhao. Auto-encoder based dimensionality reduction. *Neurocomputing*, 184:232–242, 2016. ISSN 0925-2312. doi: <https://doi.org/10.1016/j.neucom.2015.08.104>. URL <https://www.sciencedirect.com/science/article/pii/S0925231215017671>. RoLoD: Robust Local Descriptors for Computer Vision 2014.
- P. K. Yeung and M. S. Bogras. Relative dispersion in isotropic turbulence. part 1. direct numerical simulations and reynolds-number dependence. *Journal of Fluid Mechanics*, 503:93–124, 2004. doi: 10.1017/S0022112003007584.
- Xiaoming Zhai, Yue Yin, James W. Pellegrino, Kevin C. Haudek, and Lehong Shi. Applying machine learning in science assessment: a systematic review. *Studies in Science Education*, 56(1):111–151, 2020. doi: 10.1080/03057267.2020.1735757. URL <https://doi.org/10.1080/03057267.2020.1735757>.

## A Appendix: SPH (in more details)

### A.1 Basic formulation

Essentially, SPH is a discrete approximation to a continuous flow field by using a series of discrete particles. Lets first start with the identity

$$A(\mathbf{r}) = \int_V A(\mathbf{r}') \delta(\mathbf{r} - \mathbf{r}') d\mathbf{r}',$$

where  $A$  is any scalar or tensor field. Using the smoothing kernel  $W$  (for interpolation onto smooth "blobs" of fluid) and after a Taylor expansion it can be shown (according to symmetry of smoothing kernel (Cossins, 2010)) that

$$A(\mathbf{r}) = \int_V A(\mathbf{r}') W(|\mathbf{r} - \mathbf{r}'|, h) d\mathbf{r}' + \mathcal{O}(h^2).$$

where  $W$  is constrained to behave similar to the delta function,

$$\int_V W(\mathbf{r}, h) d\mathbf{r} = 1, \quad \lim_{h \rightarrow 0} W(\mathbf{r}, h) = \delta(\mathbf{r}).$$

The choice of smoothing kernels is important, and effects the consistency and accuracy of results (Monaghan, 2005), where bell-shaped, symmetric, monotonic kernels are the most popular (Fulk & Quinn, 1996), however there is still disagreement on the best smoothing kernels to use (but generally should satisfy the conditions outlined in (Liu & Liu, 2010a)). Commonly used are the B-spline smoothing kernels with a finite support (approximating a Gaussian kernel). The cubic smoothing kernel is used in this work has the following form:

$$w(q) = \sigma \begin{cases} \frac{1}{4}(2-q)^3 - (1-q)^3 & 0 \leq q < 1 \\ \frac{1}{4}(2-q)^3 & 1 \leq q \leq 2 \\ 0 & 2 \leq q \end{cases} \quad (16)$$

where,  $W(|\mathbf{r} - \mathbf{r}_j|, h) = h^{-d} w(q)$  with  $q = |\mathbf{r} - \mathbf{r}_j|/h$ , and  $\sigma = \sigma(d) = [1/\pi$  if  $d = 3$ ,  $10/7\pi$  if  $d = 2]$  is a normalizing constant to satisfy the integral constraint on  $W$  (see (Cossins, 2010; Fulk & Quinn, 1996; Monaghan, 2012) for more details). The finite support allows one to use neighborhood list algorithms discussed below to utilize computational advantages (only requires a local cloud of interacting particles instead of all the particles in the computational domain that would be required with a Gaussian kernel). The quartic smoothing kernel (see (Liu & Liu, 2010b)) used in this work is

$$w(q) = \sigma \begin{cases} (2/3 - 9/8q^2 + 19/24q^3 - 5/32q^4) & 0 \leq q < 2 \\ 0 & 2 \leq q \end{cases} \quad (17)$$

Where  $\sigma = 315/(208\pi h^3)$  for  $d = 3$ .

SPH can be formulated through approximating integral interpolants of any scalar or tensor field  $A$  by a series of discrete particles

$$\begin{aligned} \langle A(\mathbf{r}) \rangle &= \int_V A(\mathbf{r}') W(|\mathbf{r} - \mathbf{r}'|, h) d\mathbf{r}' \\ &\approx \sum_i m_i \frac{A(\mathbf{r}_i)}{\rho(\mathbf{r}_i)} W(|\mathbf{r} - \mathbf{r}_i|, h), \end{aligned} \quad (18)$$

(i.e a convolution of  $A$  with  $W$ ) where  $d\mathbf{r}'$  denotes a volume element and  $W(r, h)$  is the smoothing kernel. Each particle represents a continuous "blob" of fluid and carries the fluid quantities in the Lagrangian frame (such as pressure  $P_i$ , density  $\rho_i$ , velocity  $\mathbf{v}_i$ , etc.)

The convenience of this method becomes apparent when the differential operators are approximated (see (Liu & Liu, 2010b) for a more detailed derivation). Using the integral interpolation,

$$\langle \nabla_r A(\mathbf{r}) \rangle = \int_V \nabla_r A(\mathbf{r}') W(\|\mathbf{r} - \mathbf{r}'\|_2, h) d\mathbf{r}'.$$

Now, using the particle approximation

$$\langle \nabla_r A(\mathbf{r}) \rangle \approx \sum_i m_i \frac{A(\mathbf{r}_i)}{\rho(\mathbf{r}_i)} \nabla_r W(\|\mathbf{r} - \mathbf{r}_i\|_2, h),$$

where we see that in this direct approach to approximate the gradient operator we only need to know the gradient of the smoothing kernel (which is usually fixed beforehand). Multiple methods have been proposed and different methods are best suited for different problems. Similar approximations hold for taking the divergence or curl of a vector field (Gingold & Monaghan, 1977). The most common "symmetrized" approximation of the gradient operator is derived from the following identity,

$$\nabla_r A(\mathbf{r}_i) = \rho \left( \frac{A(\mathbf{r}_i)}{\rho^2} \nabla_r \rho - \nabla_r \left( \frac{A(\mathbf{r}_i)}{\rho} \right) \right),$$

and is approximated with particles as

$$\nabla_r A_i \approx \rho_i \sum_j^N m_j \left( \frac{A_j}{\rho_j^2} - \frac{A_i}{\rho_i^2} \right) \nabla_{\mathbf{r}_i} W_{ij}. \quad (19)$$

## A.2 Approximation of Flow Equations

The above integral interpolant approximations using series of particles can be used to discretize the equations of motion (as seen in Eq. (2) with more details found in (Gingold & Monaghan, 1977; Monaghan, 2012)). Each particle carries a mass  $m_i$  and velocity  $\mathbf{v}_i$ , and other properties (such as pressure, density etc.). We can use Eq. (18) to estimate the density everywhere by

$$\rho(\mathbf{r}_i) = \sum_j m_j W(\|\mathbf{r}_i - \mathbf{r}_j\|, h),$$

where although the summation is over all particles, because the smoothing kernel has compact support the summation only needs to occur over the smoothing radius (here  $2h$  as seen in Eq. (16)). Another popular way to approximate the density is through

using the continuity equation and approximating the divergence of the velocity field in different ways (Monaghan, 1992). In what follows we use the notation  $A_i = A(\mathbf{r}_i)$ . Using the gradient approximation defined above (Eq. (19)), the pressure gradient could be estimated by using

$$\rho_i \nabla_r P_i = \sum_j m_j (P_j - P_i) \nabla_{\mathbf{r}_i} W_{ij},$$

where  $W_{ij} = W(|\mathbf{r}_i - \mathbf{r}_j|, h)$ . However, in this form the momentum equation  $d_t \mathbf{v} = -\frac{1}{\rho} \nabla_r P$  does not conserve linear and angular momentum (Monaghan, 1992). To improve this, a symmetrization is often done to the pressure gradient term by rewriting  $\frac{\nabla_r P}{\rho} = \partial_r \left( \frac{P}{\rho} \right) + \frac{P}{\rho^2} \nabla_r \rho$ . This results in a momentum equation for particle  $i$  discretized as

$$\frac{d\mathbf{v}_i}{dt} = - \sum_j m_j \left( \frac{P_j}{\rho_j^2} + \frac{P_i}{\rho_i^2} \right) \nabla_{\mathbf{r}_i} W_{ij},$$

which produces a symmetric central force between pairs of particles and as a result linear and angular momentum are conserved (Monaghan, 1992). Next, including an artificial viscosity term and external forcing, the full set of ODEs approximating PDEs governing fluid motion (namely Euler's equations with an added artificial viscosity  $\Pi$ ) is

$$\begin{aligned} \frac{d\mathbf{r}_i}{dt} &= \mathbf{v}_i \quad \forall i \in \{1, 2, \dots, N\} \\ \frac{d\mathbf{v}_i}{dt} &= - \sum_{j \neq i}^N m_j \left( \frac{P_j}{\rho_j^2} + \frac{P_i}{\rho_i^2} + \Pi_{ij} \right) \nabla_{\mathbf{r}_i} W_{ij} + \mathbf{f}_{ext}. \end{aligned}$$

In this work, we start by using the weakly compressible formulation by assuming a barotropic fluid, where equation of state (EoS) is given by

$$P(\rho) = \frac{c^2 \rho_0}{\gamma} \left[ \left( \frac{\rho}{\rho_0} \right)^\gamma - 1 \right],$$

as in (Monaghan, 2012), where  $\rho_0$  is the initial reference density, and  $\gamma = 7$  is used. In future work, we plan on including the energy equation to extend these methods for highly compressible applications.

There are many different forms of artificial viscosity that have been proposed (Monaghan, 1997). In this work, we use the popular formulation of  $\Pi_{ij}$  that approximates the contribution from the bulk and shear viscosity along with an approximation of Nueman-Richtmyer viscosity for handling shocks (Monaghan, 2012; Morris et al., 1997):

$$\Pi_{ij} = \begin{cases} \frac{-\alpha c_{ij} \mu_{ij} + \beta \mu_{ij}^2}{\rho_{ij}}, & \mathbf{v}_{ij} \cdot \mathbf{r}_{ij} < 0, \\ 0, & \text{otherwise} \end{cases}, \quad (20)$$

where  $c_{ij} = 0.5(c_i + c_j)$  and  $c_i = \sqrt{dP(\rho_i)/d\rho}$  represents the speed of sound of particle  $i$  and

$$\mu_{ij} = \frac{h\mathbf{v}_{ij} \cdot \mathbf{r}_{ij}}{|\mathbf{r}_{ij}|^2 + \epsilon h^2}, \quad \rho_{ij} = 0.5(\rho_i + \rho_j),$$

This artificial viscosity term was constructed in the standard way following (Monaghan, 1997; Monaghan & Gingold, 1983): The linear term involving the speed of sound was based on the viscosity of an ideal gas. This term scales linearly with the velocity divergence, is negative to enforce  $\Pi_{ij} > 0$ , and should be present only for convergent flows ( $\mathbf{v}_{ij} \cdot \mathbf{r}_{ij} < 0$ ). The quadratic term including  $(\mathbf{v}_{ij} \cdot \mathbf{r}_{ij})^2$  is used to prevent penetration in high Mach number collisions by producing an artificial pressure roughly proportional to  $\rho|\mathbf{v}|^2$  and approximates the von Neumann-Richtmyer viscosity (and should also only be present for convergent flows). There are several advantages to this formulation of  $\Pi_{ij}$ ; mainly it is Galilean and rotationally invariant, thus conserves total linear and angular momentum. A more detailed derivation is found in (Cossins, 2010) (along with other formulations of artificial viscosities).

In practice the summation Eq. (2) over all particles is carried out through a neighborhood list algorithm (such as the cell linked list algorithm with a computational cost that scales as  $\mathcal{O}(N)$  (Domínguez et al., 2011)). We also note that Eq. (2) can also be derived from Euler-Lagrange equations after defining a Lagrangian, see (Cossins, 2010) (for respective analysis of the inviscid case, when the artificial viscosity term is neglected), then an artificial viscosity  $\Pi_{ij}$  term can be incorporated from using SPH discretizations, see (Monaghan, 2005) for details.

### A.3 External Forcing

In order to approach a stationary homogeneous and isotropic turbulent flow, we explored two different external forcing, stochastic and deterministic. We first use a stochastic external forcing acting on large scales which forces 10 modes that are close to the origin in Fourier space. In 2D, this is formally expressed as  $\mathbf{f}_{ext} = (f_{ext}^x, f_{ext}^y)^T$

$$\begin{aligned} f_{ext}^x[i] &= - \sum_{k=1}^{10} \cos(f_k^x x_i + f_k^y y_i + 2\pi\zeta(t, k)) \tilde{f}_k f_k^y, \\ f_{ext}^y[i] &= \sum_{k=1}^{10} \cos(f_k^x x_i + f_k^y y_i + 2\pi\zeta(t, k)) \tilde{f}_k f_k^x, \\ \tilde{f}_k &= 0.25 \left( \frac{2.5 - \sqrt{(f_k^x)^2 + (f_k^y)^2}}{1.5} \right)^2, \end{aligned}$$

where  $(f_k^x, f_k^y)$  are the frequency components that lie near to the origin (in frequency space), and  $\zeta(t, k)$  is a stochastic white noise term.

A deterministic forcing is used (for simplifying the learning algorithms), which is commonly used in CFD literature, (e.g. as in (Petersen & Livescu, 2010) which is what is used in generating the ground truth DNS data) for analyzing stationary homogeneous and isotropic turbulence. Then,

$$\mathbf{f}_{ext}^i = \frac{\theta_{inj}}{KE} \mathbf{v}_i, \quad KE = \frac{0.5}{N} \sum_{k=1}^N \rho_k (u_k^2 + v_k^2 + w_k^2)$$

is the kinetic energy computed at each time step,  $\theta_{inj}$  represents the rate of energy injected into the flow.

#### A.4 Numerical Algorithm for Forward Solving SPH

We use a Velocity Verlet (leap frog) numerical scheme for generating the SPH ground truth data, and for making prediction steps required in our gradient based optimization described in Eq. (4). Using the notation,

$$\mathbf{X} = \{(\mathbf{r}_i, \mathbf{v}_i) | \forall i \in \{1, \dots, N\}\}, \quad \boldsymbol{\rho} = \{\rho_i | \forall i \in \{1, \dots, N\}\},$$

$$\frac{d\mathbf{r}_i}{dt} = \mathbf{v}_i, \quad \frac{d\mathbf{v}_i}{dt} = \mathbf{F}_i(\boldsymbol{\rho}, \mathbf{X}),$$

we proceed according to the following algorithm

- 1: Compute  $\boldsymbol{\rho}^k$  using Eq. (18),
- 2: Compute  $\mathbf{F}_i^k(\boldsymbol{\rho}^k, \mathbf{X}^k)$  using Eq. (2),
- 3:  $\mathbf{v}_i^{k+\frac{1}{2}} = \mathbf{v}_i^k + \frac{\Delta t}{2} \mathbf{F}_i^k$ ,
- 4:  $\mathbf{r}_i^{k+1} = \mathbf{r}_i^k + \Delta t \mathbf{v}_i^{k+\frac{1}{2}}$ ,
- 5: Compute  $\boldsymbol{\rho}^{k+1}$  using Eq. (18),
- 6: Compute  $\mathbf{F}_i^{k+\frac{1}{2}}(\boldsymbol{\rho}^{k+1}, \mathbf{X}^{k+\frac{1}{2}})$  using Eq. (2),
- 7:  $\mathbf{v}_i^{k+1} = \mathbf{v}_i^{k+\frac{1}{2}} + \frac{\Delta t}{2} \mathbf{F}_i^{k+\frac{1}{2}}$ ,

repeated for each time step,  $k \in \{0, \Delta t, \dots, T\}$ , where the time step,  $\Delta t$ , is chosen according to the Courant-Friedrichs-Lewy (CFL) condition,  $\Delta t \leq 0.4h/c$ . This algorithm has the following physical interpretation: it prevents spatial information transfer through the code at a rate greater than the local speed of sound (small in the almost incompressible case considered in this manuscript).

## B Appendix: Methods

### B.0.1 Forward Sensitivity Analysis

In general, the loss functions in this work can be defined as

$$L(\mathbf{X}, \boldsymbol{\theta}) = \int_0^{t_f} \Psi(\mathbf{X}, \boldsymbol{\theta}, t) dt.$$

The forward SA (FSA) approach simultaneously integrates the state variables along with their sensitivities (with respect to parameters) forward in time to compute the gradient of  $L$ ;

$$d_{\theta}L = \int_0^{t_f} \partial_{\mathbf{X}}\Psi(\mathbf{X}, \boldsymbol{\theta}, t)d_{\theta}\mathbf{X}(\boldsymbol{\theta}, t) + \partial_{\theta}\Psi(\mathbf{X}, \boldsymbol{\theta}, t)dt. \quad (21)$$

Where, through using the chain rule, we see that the sensitivities of the state variables with respect to the model parameters ( $d_{\theta}\mathbf{X}$ ) are required to compute the gradient of the loss. Assuming that the initial conditions of the state variables do not depend on the parameters, then  $\partial\mathbf{X}(0)/\partial\theta^{\alpha} = 0$ . Now, define the sensitivities as  $\mathbf{S}_i^{\alpha} := d\mathbf{X}_i/d\theta^{\alpha}$ . Then, from Eq. (13) we derive

$$\frac{d\mathbf{S}_i^{\alpha}}{dt} = \frac{d\mathcal{F}_i(\mathbf{X}(t), \boldsymbol{\theta})}{d\theta^{\alpha}}, \quad (22)$$

then resulting, after applying the chain rule, in

$$\frac{d\mathbf{S}_i^{\alpha}}{dt} = \frac{\partial\mathcal{F}_i(\mathbf{X}(t), \boldsymbol{\theta})}{\partial\mathbf{X}_i}\mathbf{S}_i^{\alpha} + \frac{\partial\mathcal{F}_i(\mathbf{X}(t), \boldsymbol{\theta})}{\partial\theta^{\alpha}}. \quad (23)$$

Since the initial condition  $\mathbf{X}(0)$  does not depend on  $\boldsymbol{\theta}$ , then  $\mathbf{S}_i^{\alpha}(0) = 0$ . Now, computing the gradient of the loss function reduces to solving a forward in time Initial Value Problem (IVP) by integrating simultaneously the state variables  $\mathbf{X}_i$  defined in the main text, and sensitivities  $\mathbf{S}_i^{\alpha}$ , defined in Eq. (23). However, this means that the computational cost of the FSA method scales with  $\mathcal{O}(Nk)$ , where  $k$  is the number of parameters, which can be large when using NN's. However, when there are many particles, . With  $\mathbf{S}_i^{\alpha}$  known, the parameters can then be learned (estimated) through an iterative first order gradient based approach (such as by updating  $\boldsymbol{\theta}$  using adaptive moment estimation (Adam) (Kingma & Ba, 2017)) where the gradient is computed in Eq. (21).

In order to integrate Eq. (23) the gradient of  $\mathcal{F}_i$  with respect to the parameters, both  $\partial\mathcal{F}_i(\mathbf{X}(\tau), \boldsymbol{\theta})/\partial\theta^{\alpha}$  and the Jacobian matrix,  $\partial\mathcal{F}_i(\mathbf{X}(\tau), \boldsymbol{\theta})/\partial\mathbf{X}_i$  need to be computed. In this work, this is done with a mixed mode approach.  $\partial\mathcal{F}_i(\mathbf{X}(\tau), \boldsymbol{\theta})/\partial\theta^{\alpha}$ , with  $\mathcal{F}_i(\boldsymbol{\theta}) : \mathbb{R}^k \rightarrow \mathbb{R}^{2d}$ , is computed with AD (the choice of forward or reverse mode is determined by the dimension of the input and output space), where  $k$  is the number of parameters and  $d$  is the dimension. For example, if  $k \gg 2d$  (as is the case when NNs are used), reverse mode AD is more efficient than forward mode (Ma et al., 2021). The Jacobian matrix is computed and obtained through mixing symbolic differentiation packages (or analytically deriving by hand), as well as mixing AD. For example, when there are NNs used for the parameterization of the right hand side, then according to expression for the Jacobian from the main text, AD derivatives will need to be computed on different functions each with potentially different dimensions of input and output space. With  $\mathcal{F}_i(\mathbf{X}) : \mathbb{R}^{2d} \rightarrow \mathbb{R}^{2d}$ , forward mode AD is more efficient. As seen in the subsection 4.1, some of the models we train require neighborhood search list algorithms, which in this case AD is only applied to derivative within the Jacobian, especially whenever summation over particles is done. Thus, a mixed mode approach is taken by combining

both forward and reverse mode (depending on dimensions) to improve the efficiency over just applying one or the other. The AD packages used in this work were both ForwardDiff.jl (Revels et al., 2016) for forward mode and Zygote.jl (Innes, 2018) for reverse mode. For example, the Jacobian matrix for 2D problems is

$$\frac{\partial \mathcal{F}_i(\mathbf{X}(t), \boldsymbol{\theta})}{\partial \mathbf{X}_i} = \begin{pmatrix} [0]_2 & I_2 \\ \frac{\partial \mathcal{F}_i(\mathbf{X}(t), \boldsymbol{\theta})}{\partial \mathbf{X}_i} \end{pmatrix}$$

$$= \begin{pmatrix} [0]_2 & I_2 \\ \frac{\partial F_i^x}{\partial x_i^1} & \frac{\partial F_i^x}{\partial x_i^2} & \frac{\partial F_i^x}{\partial x_i^3} & \frac{\partial F_i^x}{\partial x_i^4} \\ \frac{\partial F_i^y}{\partial x_i^1} & \frac{\partial F_i^y}{\partial x_i^2} & \frac{\partial F_i^y}{\partial x_i^3} & \frac{\partial F_i^y}{\partial x_i^4} \end{pmatrix}.$$

where, the individual derivatives  $\frac{\partial F_i^y}{\partial x_i^d}$  are computed with AD (Reverse or Forward mode depending on model chosen from subsection 4.1).

## B.0.2 Adjoint Method

This section provides an outline of the Adjoint SA (ASA) method used in this work (for more details, see (Bradley, 2019) (Donello et al., 2020)). Again, the goal is to compute the gradient of the loss function. This is a continuous time dependent formulation, where the goal is to minimize a loss function  $L(\mathbf{X}(\boldsymbol{\theta}, t), \boldsymbol{\theta})$  which is integrated over time,  $L(\mathbf{X}, \boldsymbol{\theta}) = \int_0^{t_f} \Psi(\mathbf{X}, \boldsymbol{\theta}, t) dt$ , subject to the physical structure constraints (ODE or PDE),  $H(\mathbf{X}, \dot{\mathbf{X}}, \boldsymbol{\theta}, t) = 0$ , and the dependence of the initial condition,  $g(\mathbf{X}(0), \boldsymbol{\theta}) = 0$ , on parameters. Here,  $H$  is the explicit ODE form obtained through the SPH discretization equations Eq. (13) (discretization of PDE flow equations),

$$H(\mathbf{X}, \dot{\mathbf{X}}, \boldsymbol{\theta}, t) = \dot{\mathbf{X}}(t) - \mathcal{F}(\mathbf{X}(t), \boldsymbol{\theta}). \quad (24)$$

A gradient based optimization algorithm requires that the gradient of the loss function,

$$d_{\boldsymbol{\theta}} L(\mathbf{X}, \boldsymbol{\theta}) = \int_0^{t_f} \partial_{\mathbf{X}} \Psi(\mathbf{X}, \boldsymbol{\theta}, t) d_{\boldsymbol{\theta}} \mathbf{X}(\boldsymbol{\theta}, t) + \partial_{\boldsymbol{\theta}} \Psi(\mathbf{X}, \boldsymbol{\theta}, t) dt,$$

be computed. The main difference in the FSA and ASA approach is that in the ASA calculating  $d_{\boldsymbol{\theta}} \mathbf{X}$  is not required (which avoids integrating the additional  $k$  ODEs as in FSA). Instead, the adjoint method develops a second ODE (size of which is independent

of  $k$ ) in the adjoint variable  $\lambda$  as a function of time (which is then integrated backwards in time).

The following provides a Lagrange multiplier approach to deriving this ODE in  $\lambda$ . First define

$$\mathcal{L} = \int_0^{t_f} (\Psi(\mathbf{X}, \boldsymbol{\theta}, t) + \boldsymbol{\lambda}^T(t)H(\mathbf{X}, \dot{\mathbf{X}}, \boldsymbol{\theta}, t))dt + \boldsymbol{\mu}^T g(\mathbf{X}(0), \boldsymbol{\theta}),$$

where  $\lambda$  and  $\mu$  are the Lagrange multipliers. Now, since  $H$  and  $g$  are zero everywhere, we may choose the values of  $\lambda$  and  $\mu$  arbitrarily; also as a consequence of  $H$  and  $g$  being everywhere zero, we note that  $\nabla_{\boldsymbol{\theta}}\mathcal{L} = \nabla_{\boldsymbol{\theta}}L$ .

Now, taking the gradient of Eq. (25), and simplifying

$$\begin{aligned} \nabla_{\boldsymbol{\theta}}\mathcal{L} = & \int_0^{t_f} (\partial_{\mathbf{X}}\Psi d_{\boldsymbol{\theta}}\mathbf{X} + \partial_{\boldsymbol{\theta}}\Psi + \boldsymbol{\lambda}^T(\partial_{\mathbf{X}}H d_{\boldsymbol{\theta}}\mathbf{X} \\ & + \partial_{\dot{\mathbf{X}}}H d_{\boldsymbol{\theta}}\dot{\mathbf{X}} + \partial_{\boldsymbol{\theta}}H))dt \\ & + \boldsymbol{\mu}^T(\partial_{\mathbf{X}(0)}g d_{\boldsymbol{\theta}}\mathbf{X}(0) + \partial_{\boldsymbol{\theta}}g). \end{aligned}$$

Integrating the equation by parts, and eliminating,  $d_{\boldsymbol{\theta}}\dot{\mathbf{X}}$ , we arrive at

$$\begin{aligned} \nabla_{\boldsymbol{\theta}}\mathcal{L} = & \int_0^{t_f} \left[ (\partial_{\mathbf{X}}\Psi + \boldsymbol{\lambda}^T(\partial_{\mathbf{X}}H - d_t\partial_{\dot{\mathbf{X}}}H) - \dot{\boldsymbol{\lambda}}^T\partial_{\dot{\mathbf{X}}}H) d_{\boldsymbol{\theta}}\mathbf{X} \right. \\ & \left. + \partial_{\boldsymbol{\theta}}\Psi + \boldsymbol{\lambda}^T\partial_{\boldsymbol{\theta}}H \right] dt + \boldsymbol{\lambda}^T\partial_{\dot{\mathbf{X}}}H d_{\boldsymbol{\theta}}\mathbf{X} \Big|_{t_f} \\ & + (-\boldsymbol{\lambda}^T\partial_{\dot{\mathbf{X}}}H + \boldsymbol{\mu}^T g) \Big|_0 d_{\boldsymbol{\theta}}\mathbf{X}(0) + \boldsymbol{\mu}^T\partial_{\boldsymbol{\theta}}g. \end{aligned}$$

Since the choice of,  $\lambda^T$ , and,  $\mu$ , is arbitrary, we set,  $\lambda^T(T) = 0$ , and,  $\mu^T = (\lambda^T\partial_{\dot{\mathbf{X}}}H)|_0(g|_{\mathbf{X}(0)})^{-1}$ , in order to avoid needing to compute,  $d_{\boldsymbol{\theta}}\mathbf{X}(T)$ , and thus canceling the second to the last term in the latest (inline) expression. Now, assuming that the initial values of the state variables,  $\mathbf{X}(0)$ , do not depend on the parameters, then  $d_{\boldsymbol{\theta}}\mathbf{X}(0) = 0$ , and,  $g = 0$ . Furthermore, we use a loss function  $\Psi$  that does not depend on  $\boldsymbol{\theta}$  explicitly, so that,  $\partial_{\boldsymbol{\theta}}\Psi = 0$ . And finally, we can avoid computing  $d_{\boldsymbol{\theta}}\mathbf{X}$  at all other times  $t > 0$  by setting

$$\partial_{\mathbf{X}}\Psi + \boldsymbol{\lambda}^T(\partial_{\mathbf{X}}H - d_t\partial_{\dot{\mathbf{X}}}H) - \dot{\boldsymbol{\lambda}}^T\partial_{\dot{\mathbf{X}}}H = 0.$$

The resulting equation for the time derivative of  $\lambda$  can be re-stated as the following Adjoint Equation (AE)

$$\dot{\boldsymbol{\lambda}}^T = \partial_{\mathbf{X}}\Psi - \boldsymbol{\lambda}^T \frac{\partial \mathcal{F}}{\partial \mathbf{X}}, \quad \boldsymbol{\lambda}(t_f) = 0, \quad (25)$$

where we also used that according to Eq. (24),  $\partial_{\mathbf{X}}H = -\partial_{\mathbf{X}}\mathcal{F}$  and  $\partial_{\dot{\mathbf{X}}}H = I_{2d}$ .

Combining all of the above, we see that the simplified equation for the gradient of the loss function is

$$\nabla_{\theta}L = \nabla_{\theta}\mathcal{L} = \int_0^{t_f} \lambda^T \partial_{\theta}H dt.$$

Which, according to Eq. (24), becomes

$$\nabla_{\theta}L = - \int_0^{t_f} \lambda^T \frac{\partial \mathcal{F}}{\partial \theta} dt.$$

Therefore, in order to compute the gradient, the IVP expression Eq. (25) needs to be integrated backwards in time for  $\lambda(t)$ , starting from  $\lambda(t_f) = 0$ . Similar to the FSA formulation found above, both  $\partial_{\mathbf{x}}\mathcal{F}$  and  $\partial_{\theta}\mathcal{F}$ , are computed with a mixture of forward and reverse mode AD tools, depending on the dimension of the input and output dimension of the functions to be differentiated.

## B.1 Learning Algorithm

In what follows, we combine all of the computational tools and techniques introduced so far to outline the mixed mode learning algorithm.

---

### Algorithm 1: Mixed Mode Learning Algorithm

---

Given Ground Truth:  $\{\mathbf{X}(t_0), \mathbf{X}(t_1), \dots, \mathbf{X}(t_f)\}$  SPH data ;  
 Select model:  $d_t \mathbf{X}(t) = \mathcal{F}(\mathbf{X}(t), \boldsymbol{\theta})$  from hierarchy  
 Select SA method (Forward or Adjoint)  
 Choose Loss methods (combination of Trajectory, Field, or Probabilistic)  
 Choose optimizer: e.g  $Opt = \{RMSprop, ADAM\}$   
**for**  $k \in \{1, \dots, n\}$  **do**  
   Prediction step: Verlet integration of model  $\hat{\mathbf{X}} = Verlet(\mathcal{F}, \boldsymbol{\theta}_k, \mathbf{X}(t_0), t_0, t_f)$   
   Simultaneously computes  $\frac{\partial \mathcal{F}}{\partial \hat{\mathbf{X}}_i}, \frac{\partial \mathcal{F}}{\partial \boldsymbol{\theta}}$  with mixed mode AD.  
   **if** Forward SA **then**  
     Simultaneously integrate system of ODEs for sensitivities  $\mathbf{S}_i^\alpha$ ;  
     
$$d_t \mathbf{S}_i = \frac{\partial \mathcal{F}_i(\hat{\mathbf{X}}(t), \boldsymbol{\theta}_k)}{\partial \hat{\mathbf{X}}_i} \mathbf{S}_i + \frac{\partial \mathcal{F}_i(\hat{\mathbf{X}}(t), \boldsymbol{\theta}_k)}{\partial \boldsymbol{\theta}_k}$$
  
     Compute  $\nabla L$   
   **else if** Adjoint SA **then**  
     Integrate  $d_t \boldsymbol{\lambda}^T$  backwards in time (store forward solve);  
     
$$d_t \boldsymbol{\lambda}^T = \partial_{\hat{\mathbf{X}}} \Psi - \boldsymbol{\lambda}^T \frac{\partial \mathcal{F}}{\partial \hat{\mathbf{X}}}, \quad \boldsymbol{\lambda}(t_f) = 0$$
  
     Compute  $\nabla L$   
   **end**  
   Obtain predicted probability distribution  $\hat{G} = KDE(\hat{\mathbf{z}})$   
   update  $\boldsymbol{\theta}$  using optimizer;  
    $\boldsymbol{\theta}_{k+1} = Opt(\boldsymbol{\theta}_k)$   
**end**  
**Result:** Estimates  $\hat{\boldsymbol{\theta}}$  so that Lagrangian model is fitted to SPH data with locally minimized loss

---

## C Additional SPH training data Results

To compute the rotational and Galilean errors as seen in Table 2, we compute with the following

$$\frac{\|\mathbf{F}_{\hat{\theta}}(\mathbf{R}\mathbf{X}) - \mathbf{R}\mathbf{F}_{\hat{\theta}}(\mathbf{X})\|_F}{\|\mathbf{F}_{\hat{\theta}}(\mathbf{X})\|_F}$$

and

$$\frac{\|\mathbf{F}_{\hat{\theta}}(\mathbf{V} - \mathbf{s}) - \mathbf{F}_{\hat{\theta}}(\mathbf{V})\|_F}{\|\mathbf{F}_{\hat{\theta}}(\mathbf{V})\|_F}$$

respectively, where  $\mathbf{R}$  is a  $90^\circ$  rotation matrix,  $\mathbf{s}$  is a random shift, and  $\mathbf{F}_{\hat{\theta}}$  is the learned acceleration operator (parameterized by the learned parameters  $\hat{\theta}$ ).

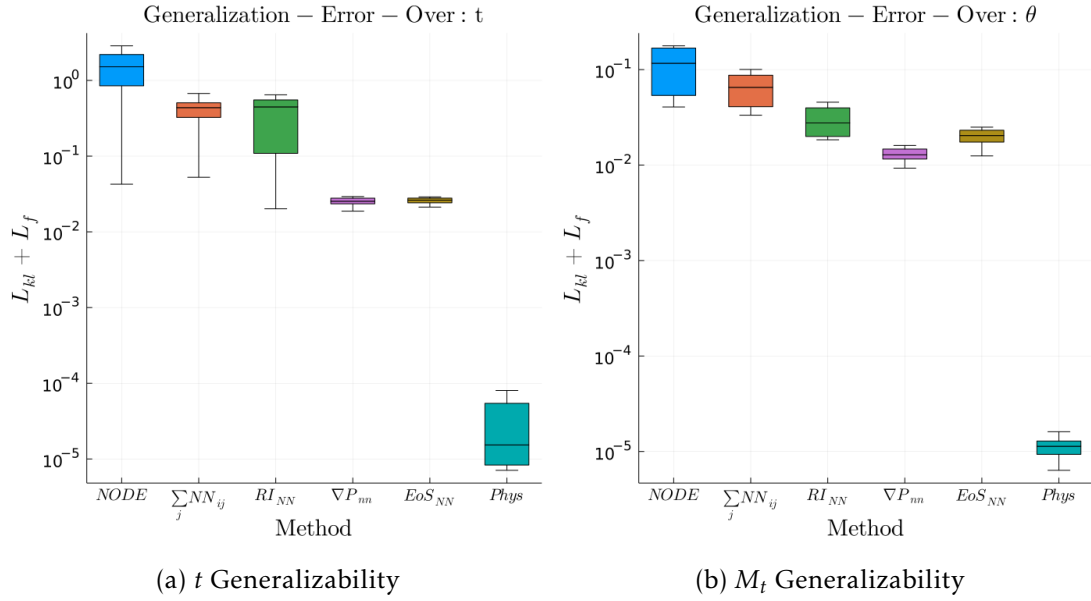


Figure 21: Additional 3D SPH training data results: (a) Box plot using 15 different generalization errors over physically relevant time scales ranging from the shortest,  $t_\lambda$  up to longest  $t_{eddy}$  (b) Box plot over 5 different generalization errors over different  $M_t$ , ranging in values up to 3 times larger than training data where the time scale is fixed at  $t_\lambda$ . Showing a robustness to learning on different flow conditions.

## D Additional DNS results: Training on $M_t = 0.16$

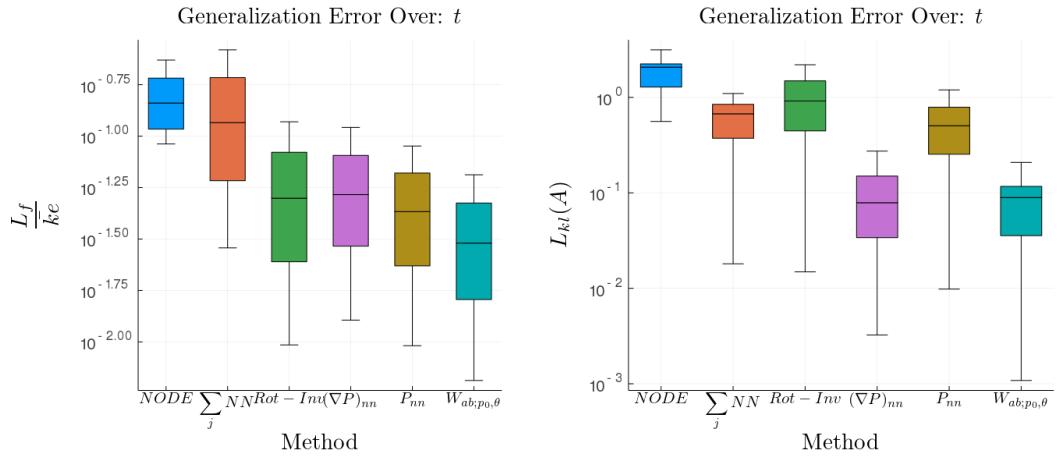


Figure 22: Training on  $L_f$  up to the Kolmogorov time scale, then comparing generalization error over longer time intervals; on the order of eddy turn over time using the field based loss. Using kl based loss on field data and statistical data:  $L_{kl}(A)$  is measuring KL divergence on acceleration distributions, and  $L_{kl}(\delta V)$  is measuring KL divergence on velocity increment distribution. This result shows that even when the models are trained on different data sets, the parameterized smoothing kernel model performs best (indicating a robustness of learning in different regimes).